Evaluation of the anisotropic grain boundaries and surfaces of α-U via molecular dynamics

Khadija Mahbuba[a], Benjamin Beeler[a,b], Andrea Jokisaari[b]

[a] *North Carolina State University, Raleigh, NC 27607*
[b] *Idaho National Laboratory, Idaho Falls, ID 83415*

Abstract

Alloys based on uranium-zirconium are gaining renewed interest as fuels for the Versatile Test Reactor and a number of microreactor designs. Implementing metallic fuel in reactors creates the need for robust descriptive and predictive fuel performance modeling. The current state of metallic fuel performance modeling relies on empirical equations derived from historical experiments, which may be unreliable when applied outside of their temperature, power, and composition phase space. One area where such data is lacking is the irradiation behavior of α-U, specifically tearing and porosity formation at early stages of irradiation. While grain boundaries likely play a key role in this fuel behavior, relatively little is known about grain boundaries in α-U. Thus, we evaluate the grain boundary, surface energy, and work of adhesion of α-U utilizing molecular dynamics. Symmetric tilt grain boundaries (STGBs) are analyzed with the tilt plane oriented along each individual major crystallographic axis, for a total of eighty unique grain boundaries. The effect of temperature, tilt plane, and misorientation angle on interfacial energies are analyzed. The interfacial energies typically increase with temperature and there is significant variance as a function of misorientation angle, irrespective of the tilt plane. At 500 K, the average surface energy (1.24 J/m^2) is approximately 1.5 times the GB energy (~~0.82~~ 0.78 J/m^2), and the WAd is approximately twice the GB energy (1.67 J/m^2). Orientations for likely formation of twins and likely cleavage planes are identified.

1. Introduction

Two life-limiting phenomena in metallic fuels are fission gas release and fuel-clad chemical interaction (FCCI) [1]. Both of these phenomena are affected by fuel swelling, which is driven by the development of porosity and fission gas bubbles. Fuel swelling in U-Zr metallic fuel is anisotropic and highly dependent upon the phase of U [2]. Within metallic fuel, it is expected that all three U allotropes are present due to both the temperature gradient across the fuel slug and the alloying composition. The low-temperature allotrope of U, α-U, is stable up to 935 K [3] and has a low symmetry orthorhombic structure with four atoms in the unit cell, as shown in Figure 1 [4].

The (0 0 1) plane of α-U can be considered to be a distorted body-centered cubic (bcc) (1 1 0) plane, where alternate parallel bcc (1 1 0) planes are offset by a distance of 2y along the $\langle 0\ 1\ 0 \rangle$ axis, where y is an internal coordinate [5]. This geometry has two mirror symmetries with respect to the (1 0 0) and (0 0

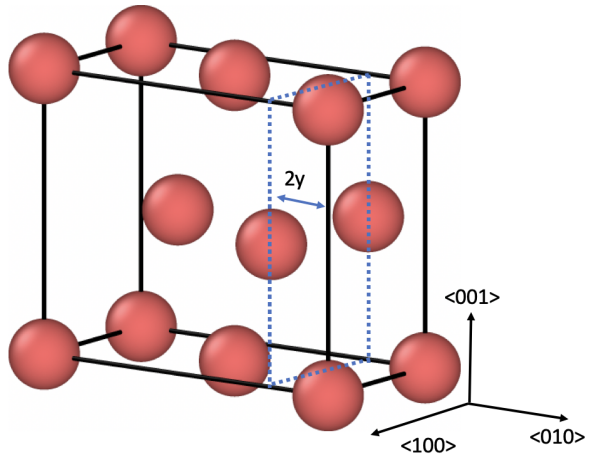

Figure 1: Orthorhombic α-U unit cell [4], which has mirror symmetry with respect to the (100) and (001) planes among the three major planes. The (0 0 1) plane is similar to the (1 1 0) plane of a bcc structure where alternate bcc (1 1 0) planes are offset by 2y distance

1) planes [6, 7, 8]. Because of its unique crystal structure, α-U exhibits anisotropic material properties, for example, thermal expansion [9] and elastic constants [10]. α-U has a negative thermal expansion coefficient in the $\langle 0\ 1\ 0 \rangle$ direction from 300 K to 923 K [9], which is probably the result of anisotropy and the temperature dependence of elastic properties. Furthermore, single crystal α-U experiences irradiation-induced growth without a significant change in volume, in which a crystal macroscopically enlarges in the $\langle 0\ 1\ 0 \rangle$ direction and shrinks in the $\langle 1\ 0\ 0 \rangle$ direction [11]. The irradiation growth appears to be much larger at cryogenic temperatures than at 293 K, but its behavior at elevated temperatures (e.g., 700 K) is still unknown [11].

Polycrystalline α-U displays complex behavior due to the fundamental anisotropy of the crystal structure and the presence of internal microstructure [12]. Because grain boundaries (GBs) act as sinks for irradiation-induced point defects and also hinder dislocation movement, they are a very important feature affecting the deformation and plasticity of α-U. A common type of GB is a symmetric-tilt grain boundary (STGB), which has a mirror symmetry across the tilt plane with some amount of atomic misfit. Twinning is a special STGB in which there is a minimal atomic misfit across the GB plane [13, 14], typically resulting in a very low grain boundary energy [15]. Generally, low symmetry materials, such as α-U, magnesium, and beryllium, deform via several distinct modes of dislocation slip and twinning, and the relative activation of these slip modes is sensitive to grain orientation and temperature [16, 17]. However, to the authors' knowledge, no work is available on the properties of STGBs in α-U, although some research has been performed on twinning.

The earliest experimental work on the deformation of α-U via twinning was conducted in the early 1950s [7, 8, 18, 19]. Through a detailed crystallographic analysis of deformation twinning, forty-one possible twins of α-U [20] were found. It has also been observed that twins possessing a low shear factor (less than 1) are the most prominent [8, 18, 7, 20]. To date, the two most prominent twinning modes have been observed to be the $\{1\ 3\ 0\}\langle 3\ \bar{1}\ 0 \rangle$ and the $\{1\ 7\ 2\}\langle 3\ \bar{1}\ 2 \rangle$ [18, 20, 21, 22]. Though $\{1\ 1\ 2\}\langle 3\ \bar{7}\ 2 \rangle$ twins have the same

shear factor as $\{1\ 7\ 2\}\langle 3\ \bar{1}\ 2\rangle$, they exhibit a low prevalence in experimental investigations of polycrystalline α-U [18, 20, 22, 23]. Additional twin modes with orientations of $\{2\ 1\ 0\}$ and $\{1\ 7\ 6\}$ have been discovered with electron microscopy techniques [24, 25]. Though the $\{1\ 1\ 0\}$ twin has a low shear factor, it typically does not appear experimentally because this shear plane also acts as one of the dominant slip systems [20].

The effect of grain boundaries on the swelling of polycrystalline α-U remains largely unknown. It has been observed that grain boundary tearing is responsible for 50% of the reported fuel swelling [26]. Cavitational swelling at low temperatures is related to the anisotropic growth of α-U and appears to be related to twinning [2], which we emphasize, is a special type of STGB. These cavities primarily form at grain boundaries and junctions, especially at twin boundaries and junctions [27]. Though twin boundaries are not a preferable nucleation site for recrystallization, the nucleation of recrystallized grains is highly correlated with high-angle grain boundary locations [28].

The energy cost to make a cavity along the grain boundary can be expressed as the energy required to break the bonds between two existing grains [29]. This energy is called the work of adhesion (WAd), or cleavage energy, and can be interpreted as the energy difference of a STGB versus two surfaces of the same orientation. Work of adhesion is important to know how much normal stress a grain boundary can withstand [30]. Thus, the surface energy is also required to evaluate the mechanical performance of α-U. Experimental and computational studies report that the surface energy can vary from 0.5 J/m^2 to 2.5 J/m^2 [5, 31, 32, 33]. However, none of these studies were thorough in their surface orientation examinations. Most recently, density functional theory was used to calculate the surface energy of seven unique surfaces, and energies ranged from 1.756 J/m^2 to 2.151 J/m^2 [34]. This study examined a subset of potential surfaces and provides a qualitative sense of the magnitude of surface energies in α-U, but is far from a complete data set.

The ability to predict the microstructural evolution of α-U under irradiation and subjected to temperature gradients relies on an accurate understanding of interfacial properties, including GB and surface energies. Such energetic properties can serve to provide fundamental insight into the expected fission gas bubble behavior, interfacial orientations, GB mobility, and cleavage. Molecular dynamics is a powerful tool to analyze the interfacial energy, given the availability of a suitable interatomic potential [29, 35]. The current work performs a computational analysis to evaluate the GB energy and surface energy related to STGBs by molecular dynamics. Interfacial energies are determined as a function of temperature (300 K, 400 K, 500 K and 600 K) and misorientation angle. Finally, using grain boundary energies and corresponding surface energies, the work of adhesion for different STGBs is evaluated.

2. Computational Details

The Large-scale Atomic/Molecular Massively Parallel Simulator (LAMMPS) [36] is utilized to perform molecular dynamics (MD) simulations. ~~To~~ Authors have prepared the STGB geometry by two methods. In method 1, to generate the supercell, a simulation box is selected and divided into two regions. Region one is tilted by $\theta/2$, without distorting the lattice of α-U, with respect to the defined tilt axis, where θ is the

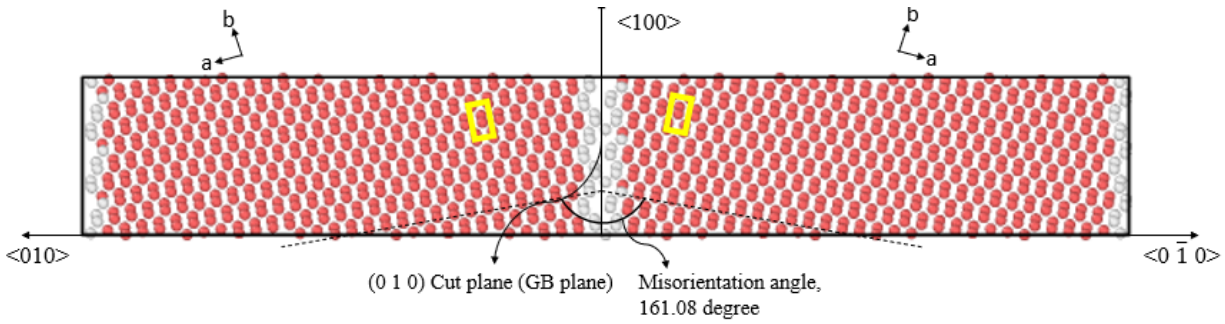

Figure 2: The as-constructed α-U symmetric-tilt grain boundary (STGB) $(\bar{1}\ 12\ 0)\langle 1\ 0\ 0\rangle$ with respect to the (0 1 0) tilt plane (or cut plane). Grain boundaries exist in the middle and on the edges of the super cell. Here the (0 0 1) plane is the shear plane. Both red and white atoms are U, but with different coordination environments to illustrate grain boundaries. Yellow rectangles indicate the α-U unit cell and a and b represent the original $\langle 1\ 0\ 0\rangle$ and $\langle 0\ 1\ 0\rangle$ crystal structure orientation.

misorientation angle and the tilt axis is parallel to the tilt plane (or cut plane). Taking the reflection of the former region across the tilt plane, region two is created, and, in the process, two symmetric tilt GBs are generated; one in the center of the supercell, and one across the periodic boundary normal to the tilt plane. To generate the surface, region two (or the mirrored region) of the supercell is considered vacuum. In this work, we utilize a STGB nomenclature of $(h\ k\ l)\langle$p q r$\rangle$, where $(h\ k\ l)$ is the misorientation plane and $\langle$p q r$\rangle$ is the tilt axis.

An as-constructed STGB plane $(\bar{1}\ 12\ 0)\langle 1\ 0\ 0\rangle$ is shown in Figure 2. In this Figure, (0 1 0) is the tilt plane (or cut plane), the left hand side of the supercell is tilted 80.54° with respect to the $\langle 1\ 0\ 0\rangle$ tilt axis, and the right-hand side is the mirror of left-hand side. Here, tilting follows the right hand rule, where (0 0 1) is the shear plane (parallel to the drawing surface) and the STGB is produced at the (0 1 0) plane (perpendicular to the drawing surface). OVITO is utilized for visualization [37].

The size of the supercell depends on the orientation of the STGB plane or surface investigated, which is selected such that the two grain boundary planes or surfaces present within a single supercell are non-interacting while also satisfying periodic boundary conditions in all directions. Thus, the number of atoms varies by grain boundary geometry, ranging from 968 to 4,800 atoms. System sizes were observed to be converged with respect to interfacial energy. A total of eighty STGBs were constructed: with twenty-four STGBs with tilt axis $\langle 1\ 0\ 0\rangle$ and shear plane (0 0 1), twenty-four with tilt axis $\langle 0\ 0\ 1\rangle$ and shear plane (0 1 0), and thirty-two with tilt axis $\langle 0\ 0\ 1\rangle$ and shear plane (1 0 0), such that a broad scope of STGBs are investigated with respect to the three crystallographic primary shear planes. Grain boundaries (or surfaces) of $(h\ k\ 0)\langle 1\ 0\ 0\rangle$, $(h\ 0\ k)\langle 0\ 0\ 1\rangle$, and $(0\ h\ k)\langle 0\ 0\ 1\rangle$ series are named as type A, B, C, respectively, and shown in the Appendix (Figure 10). Grain boundaries and surfaces, along with their misorientation angle and tilt axis are listed in the Appendix (Table 1 and Table 2, respectively). For simplicity of construction of STGBs only, the lattice parameters of α-U are considered as a=3, b=6, c=5 Å, instead of the equilibrium lattice

parameters of a=2.8, b=5.8, c=4.9 Å[4]. However, sufficient relaxation of the system is performed to ensure equilibrated systems, with equilibrium lattice constants, for the analysis of stable grain boundaries. Due to the utilization of an NPT ensemble with periodic boundaries and independent relaxation of each lattice vector, the imposed stresses from the simulation setup are rapidly relaxed. Individual unit cells from the grain interior were analyzed to ensure equilibrium lattice constants were present.

In method 2, two relaxed grains (each with two open surfaces) which are mirrored to one another with respect to tilt plane are merged together at the tilt plane and then relaxed in a NPT ensemble for 200 ps. Periodic boundary condition is applied in all direction. As the grains are already equilibrated in a NPT ensemble before merging, the lattice constants are also equilibrated at the defined temperature rather than the simplified lattice constant used in method 1. Only a subset of seven STGBs are generated in this method to compare the GB energy and radial distribution function (RDF) of respective STGBs generated in method 1. It has been observed that for some STGBSs method 1 over-predict the GB energy and for some method 2. However, discrepancy between two methods is limited to maximum 15%. Another method of calculating GB energy is γsurface method, which is not utilized in the current work. As above 0K temperature atoms at GB reorients to its relaxed orientation if sufficient relaxation time is provided, so this method is less effective at higher temperature [38].

The UMo angular dependent potential (ADP) from Ref. ~~[39]~~ [40] is used in this work. This interatomic potential reasonably predicts a number of properties in α-U, γ-U, and γ-UMo alloys. A Nose-Hoover barostat is considered for the anisotropic relaxation of the system in all directions with a damping factor of 0.1. For temperature control, a Langevin thermostat is utilized with a relaxation time of 0.1 ps. The system is observed at temperatures of 300 K, 400 K, 500 K, and 600 K, where U is present in the α phase. When the volume and energy of the system reach equilibrium, the values of observable parameters (energy and volume) are collected. Systems are equilibrated for 200 ps, and energies are averaged over the final 50 ps. To ensure statistical significance, each system is simulated three to five times, each with a unique initial distribution of velocities. This yields an maximum standard error of approximately 5% for interfacial energies.

The interfacial energies are calculated as

$$E_{\text{inf}} = \frac{E^* - E_0}{A} \times N \tag{1}$$

where E_{inf} is the interfacial (STGB or surface) energy per unit interface (STGB or surface) area, E^* is the internal energy per atom of a system with an interface, N is the number of atoms in the system with an interface, E_0 is the internal energy per atom of a defect-free system, and A is the total area of the interface (there are two interfaces per supercell). Another important parameter for micro-stucture evaluation of a polycrystalline system is the change in free energy of GB, ΔG. While calculating the ΔG at zero pressure condition, additional entropy change term, ΔS is required along with E_{inf}. ΔS can be implicitly calculated from E_{inf} at different temperature. [41]. STGBs with very low energies as per definition [13] will be considered as preferable twinning orientations, and rest of the STGBs as general STGBs in the follwing sections.

GB energies are varied with misorientation angles. Misorientation angles considered in the current work are classified into two domains, one is 0° to 180° and another is 180° to 360°. Ss all of the three investigated shear planes have a symmetry of 180°, so theoretically trend of GB energy with misorientation angle should have mirror symmetry with respect to (1 0 0), (1 0 0) and (0 0 1) planes in type A, B, and C STGBs respectively. The reason behind the two domains is to validate the result with theory. In addition, the work of adhesion of STGBs is calculated as

$$W_{\text{ad}} = 2 \times E_{\text{inf(surface)}} - E_{\text{inf(STGB)}} \tag{2}$$

where $E_{\text{inf(surface)}}$ is the surface energy per unit area and $E_{\text{inf(STGB)}}$ is the GB energy per unit area.

3. Results and Discussions

3.1. Grain Boundary Energies

3.1.1. Effect of misorientation angle

The GB energy calculated for all eighty STGBs is plotted as a function of misorientation angle in Figure 3 at 500 K. Each type of STGB (A, B, and C) has been studied for misorientation angles from 0° to 360°. As per methodology section only STGBs with misorientation angle of 0° to 180° is discussed in the following sections. There is no data available in the literature that could be explicitly compared with the result of the current work. Data points are connected by straight lines to guide the eye.

Type A STGBs ($\langle 1\ 0\ 0\rangle$ tilt axis) have deep cusps at the (0 1 0) ~~, (~~(similar (0 $\bar{1}$ 0) plane) and ($\bar{3}$ 12 0) (also similar ($\bar{3}$ $\overline{12}$ 0) ~~, and (0 $\bar{1}$ 0)~~ plane) plane, with corresponding GB energies of 0.36 J/m^2 ~~, 0.30~~ and 0.27 J/m^2~~, and 0.36 J/m^2~~. At 0° and 360°, both regions (tilted and mirror of tilted) of the supercell have their major axis ($\langle 1\ 0\ 0\rangle$ and $\langle 0\ 1\ 0\rangle$) parallel to their respective axes of the supercell. As α-U does not have a mirror symmetry with respect to the (0 1 0) plane, a GB is created at the junction of two regions, albeit with a small atomic misfit. Thus, the (0 1 0) and (0 $\bar{1}$ 0) orientations have a cusp in the GB energy profile. At the 180° misorientation, both sides (or regions) have their $\langle 010\rangle$ axis parallel to the $\langle 1\ 0\ 0\rangle$ axis of the supercell. Because of the symmetry of the (1 0 0) plane of α-U, this orientation does not describe any GB and is instead the pure crystalline system, resulting in zero grain boundary energy. ~~Type A STGBs also have a minor cusp at plane ($\bar{3}$ 6 0) with a GB energy of 0.75 J/m^2.~~ As seen in Figure 3(a), the highest GB energy is 0.9 J/m^2, which occurs at the 14.25° misoriented STGB ($\overline{12}$ 3 0)$\langle 1\ 0\ 0\rangle$. ~~If the deep cusps at the ($\bar{3}$ $\overline{12}$ 0), (0~~ GB energy increases upto 15 ° misorientation angle, followed by a decrease till 180 °, ignoring the cusp. The shape of the GB energy vs. misorientation angle has a mirror symmetry with respect to (1 0 ~~), and (0$\bar{1}$ 0) planes are ignored, type~~) plane. Type A STGBs have an average grain boundary energy of ~~0.78~~ 0.71 J/m^2, as obtained by simple averaging. Because the lowest GB energy among the type A STGB is the ($\bar{3}$ ~~$\overline{12}$~~ 12 0)$\langle 1\ 0\ 0\rangle$ orientation, it would be a likely candidate to form twins. Without considering the major cusps (very low energy STGBs), average GB energy of general STGBs results as 0.78 J/m^2. It has been experimentally observed that in α-U, grains are always oriented in a direction that is more than 60°

from the ⟨1 0 0⟩ direction (i.e. around the ⟨0 1 0⟩ direction) in pure α-U [42]. We show that STGBs tilted with respect to the ⟨1 0 0⟩ axis between ~~68.2~~63.4° to ~~111.8~~116.6° have very low energies (~~0.64~~ 0.23 J/m^2 to 0.72 J/m^2, which is equal or lower than the average GB energy compared to other STGBs of type A. This seems to support the previous experimental findings.

The grain boundary energy of type B STGBs (⟨0 0 1⟩ tilt axis) has a minor cusp at the ($\bar{2}$ 0 ~~$\bar{1}$) plane~~ 1) plane (similar to ($\bar{2}$ 0 $\bar{1}$)⟨0 0 1⟩ STGB) with a corresponding GB energy of 0.58 J/m^2. The highest GB energy for type B STGBs has been observed at the ($\bar{1}$ 0 4)⟨0 0 1⟩ ~~and ($\bar{1}$ 0 $\bar{4}$)⟨0 0 1⟩ orientations, and their respective values are~~ with a values of 0.89 J/m^2 ~~and 0.88 J/m^2.~~ . GB energy of type B STGBs becomes maximum when grains are oriented between 20° to 40° angle tilted from ⟨0 0 1⟩ axis. It should be noted that, maximum planer density for (h 0 k) surfaces is obtained at tilt angle 31 °, see Figure 10 from Appendix. At 0°, 180°, and 360° misorientations, the ⟨0 0 1⟩ axis of supercell is parallel to ⟨1 0 0⟩, ⟨0 0 1⟩, and ⟨1 0 0⟩ axis of both regions of supercell, respectively. These orientations do not create any grain boundary due to the symmetry of the (1 0 0) and (0 0 1) planes of α-U. That is why there are major cusps with a value of zero located at these orientations. Type B STGBs have a simple arithmetic average GB energy of 0.75 J/m^2. ~~Ignoring the minor cusp, this~~ This type has a mirror symmetry of STGB energy profile with respect to the (1 0 0~~1) plane~~) plane similar to type A STGB, see Figure 3(b) ~~.~~ and (a). And this phenomenon complies with the theory.

Type C STGBs (⟨0 0 1⟩ tilt axis) have the highest number of cusps (eight), which are oriented at a mirror symmetry orientation with respect to the ⟨0 0 1⟩ tilt axis, see Figure 3(c) ~~.~~ over the 0° to 360° misorientation angle domain. Apart from the mirror symmetry there is no decernible trend for GB energy of type C STGB is observerved. In the 0° to 180° misorientation angle domain, the major cusp is at the (0 1 0) and (0 18 $\overline{25}$) planes, and minor cusps exist at the (0 36 $\overline{25}$) and (0 12 $\bar{5}$) planes. The corresponding GB plane energies are 0.36 J/m^2, 0.40 J/m^2, ~~0.81 J/m^2, and~~ 0.79 J/m^2, ~~respectively. The minor cusps found in the domain of the 180° to 360° misorientation angles are the (0 $\overline{12}$ $\bar{5}$), (0 $\overline{36}$ $\overline{25}$), and (0 $\overline{36}$ $\overline{33}$) planes, which have GB energies of 0.81~~ and 0.8 J/m^2, ~~0.77 J/m^2, and 0.84 J/m^2, respectively. In the 180° to 360° domain, plane (0 $\bar{1}$ 0) has a major cusp.~~ respectively. The (0 1 0) and (0 $\bar{1}$ 0) orientations have misorientation angles of 0° and 360°, respectively, and because of α-U having no mirror symmetry with respect to the (0 1 0) plane, these planes contain GBs with a very small atomic misfit. ~~The highest GB energyamong type C STGBs is found at the~~ Because of the low GB energy, (0 ~~$\overline{18}$~~ 18 $\overline{25}$)⟨0 0 1⟩ ~~orientation, at a magnitude of 1.39 J/m^2.~~ STGB could be a probable twinning orientation of α-U. No statistically significant highest GB energy among type C STGBs is found. Like type A, at the 180° misorientation angle there is no grain boundary and zero GB energy because of the symmetry of the (0 0 1) plane of α-U. Type C STGBs have an average GB energy of ~~0.94~~ 0.89 J/m^2 considering all the cusps. ~~This value increases only by 0.04~~ Excluding the major cusps (probable twinning orientations), average GB energy of the general type C STGBs is 0.96 J/m^2~~if all the major cusps and the highest GB energy planes are excluded from the average calculation~~.

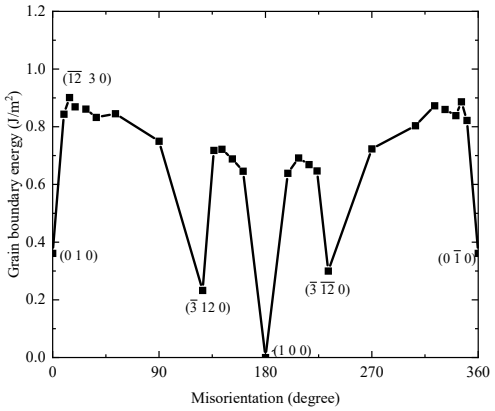

(a)

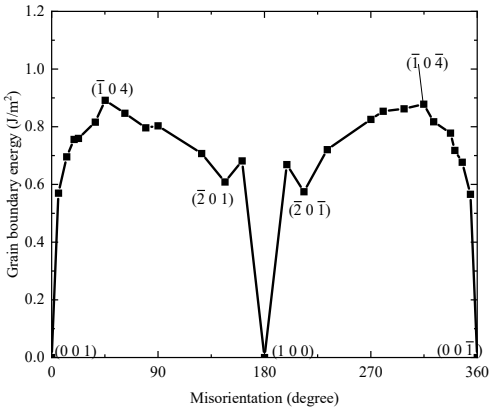

(b)

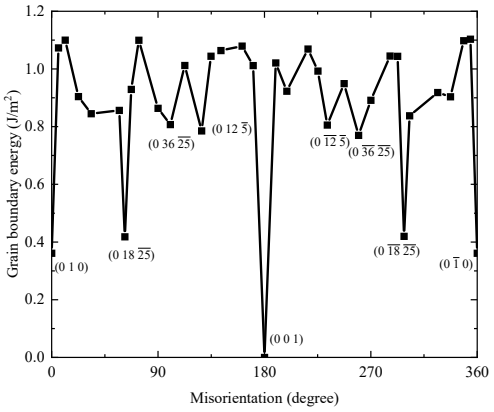

(c)

Figure 3: Grain boundary energy of STGB (symmetric tilt grain boundary) of (a) type A, (b) type B, and (c) type C as a function of misorientation angles at 500 K. Key features are labeled with their STGB plane orientation.

This study indicates that general type C STGBs have the highest average GB energy, followed by general type A STGBs, with type B STGBs exhibiting the lowest grain boundary energies. Among the entire dataset of eighty STGBs, the lowest GB energy is observed for the type A STGB at the $(\bar{3}\ \bar{12}\ 12\ 0)\langle 1\ 0\ 0\rangle$ STGB plane, where (0 1 0) is the tilt plane, (0 0 1) is the shear plane, and the GB energy is 0.30 0.27 J/m^2 . The highest GB energy is found for followed by a type C STGB at the $(0\ \bar{18}\ 18\ \bar{25})\langle 0\ 0\ 1\rangle$ STGB plane, where (0 1 0) is the tilt plane, (1 0 0) is the shear plane, and the GB energy is 1.39 0.42 J/m^2. These two could be a probable twin orientation for α-U, though none of them have

As no data on GB energies in α-U are available for comparison, the current computational work is compared with previous computational studies of γ-U, U_3Si_2, and UO_2. γ-U has a BCC crystal structure, while U_3Si_2 has a somewhat complex two sublattice tetragonal structure, and UO_2 has a fluorite structure. γ-U [43] was found to have a lower grain boundary energy than U_3Si_2 [41] at 600 K for the misorientation domain 0° to 90°. For this orientation region and temperature (analogous to the type A STGB in this work), γ-U has a GB energy from 0.3 J/m^2 - 0.45 J/m^2, whereas U_3Si_2 has a GB energy in the range of 0.7 J/m^2 - 1.2 J/m^2. Under the same conditions, α-U STGBs possess a GB energy from 0.35 J/m^2 - 0.75 J/m^2. Thus, there are good quantitative comparisons for GB energies amount these three U-based systems. At 300 K, ceramic UO_2 has a GB energy between 1.0 and 3.0 J/m^2, for a range of misorientation angles of 10° to 62° [30]. From the present work at 300 K (shown in the subsequent section), α-U shows an average GB energy of approximately 0.81 J/m^2. Hence, compared to UO_2, α-U STGBs exhibit significantly lower GB energies at 300 K.

From Fig. 3, it is observed that the GB energy of α-U not only depends on the misorientation angle, but also on the tilt plane and shear plane. This variation in GB energy is quantified here as the grain boundary anisotropy. Equation 3 refers to GB energy anisotropy (A_{TYPE} $GBAniso_{\mathrm{TYPE}}$) for a fixed misorientation angle (θ), comparing the three types of GBs, and Equation 4 compares all misorientation angles (θ) for a given type of GB to evaluate GB anisotropy (A_θ $GBAniso_\theta$) due to variation of misorientation angles.

$$AGBAniso_{\mathrm{TYPE}} = \left(\frac{max(GB_E) - min(GB_E)}{max(GB_E)}\right)_\theta \tag{3}$$

$$AGBAniso_\theta = \left(\frac{max(GB_E) - min(GB_E)}{max(GB_E)}\right)_{\mathrm{TYPE}} \tag{4}$$

To compare the dependency of the GB anisotropy on GB types (A_{TYPE}), six seven misorientation angles (9012.8°, 126.8735.7°, 161.0860°, 198.9390°, 233.13126.9° and 270, 144.3° and 161.08°) are considered for each of the three types of STGBs (Figure 4). For instance, STGB $(\bar{3}\ 6\ 0)\langle 1\ 0\ 0\rangle$ from type A, STGB $(\bar{3}\ 0\ 5)\langle 0\ 0\ 1\rangle$ from type B, and STGB $(0\ 6\ \bar{5})\langle 0\ 0\ 1\rangle$ from type C, all have the same misorientation angle of 90°. Maximum and minimum GB energy of these three planes are considered in order to evaluate the anisotropy in GB energy for the 90° misorientation due to the change in the tilt plane and shear plane (STGB type). It can be seen that as the misorientation angle increases, the anisotropy across grain boundary types decreases increases (Figure 4). Thus, at high misorientation angle, the type of tilt and shear axes are less more critical in determining the grain boundary energy. This is a general relationship, and likely does not hold for special

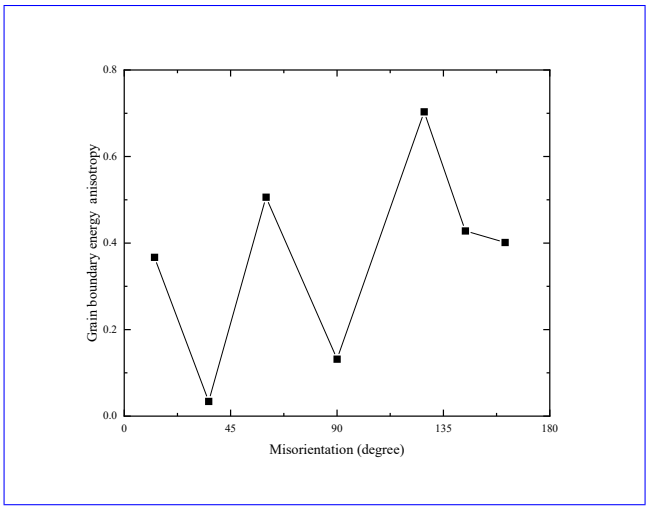

Figure 4: Grain boundary energy anisotropy (~~A~~GBAniso$_{\mathrm{TYPE}}$) in selected STGBs of α-U at 500 K. Anisotropy here is considered as a function of GB type (type A STGB, type B STGB and type C STGB).

cusps in the grain boundary landscape. At the cusp orientations (60° and 126.9°) $GBAniso_{\mathrm{TYPE}}$ becomes very large, as cusps (or preferred twinning orientations) for all types of STGBs are not formed at same misorientation angle due to anisotropic structure of α-U.

To determine the GB energy anisotropy for a fixed STGB type (for instance, type A STGBs) due to change in misorientation angle (~~A_θ~~$GBAniso_\theta$), all twenty six type A STGBs considered. Maximum and minimum GB energy are input into Equation 4, yielding three data points (one for each type STGB). The lowest anisotropy among the STGB types due to variation has been found in type B STGBs, with a value of 0.4, while type A and type C display a comparable amount of anisotropy (approximately 0.7). This qualitatively corresponds to the number of cusps and their magnitude, as observed in Figure 3. Typically, there exists a greater degree of GB energy anisotropy due to misorientation angle, rather than the underlying tilt and shear axes.

To grasp the mechanisms governing the anisotropic grain boundary properties, we must approach the problem from the perspective of the unique crystal structure of α-U. From a crystallographic point of view, α-U consists of corrugated planes parallel to the (0 1 0) plane. These corrugated planes are compressed with respect to the $\langle 0\ 0\ 1 \rangle$ direction, meaning that the corrugation direction is $\langle 0\ 0\ 1 \rangle$ and $\langle 1\ 0\ 0 \rangle$ is the transverse direction of corrugation. When (1 0 0) is designated as the shear plane (type C) to generate a STGB, continuity of the corrugated planes at the interface (or tilt plane (0 1 0)) is interrupted. As a result, at the interface, all bonds in the corrugated direction are broken and need to be reconstructed. For type B STGBs, corrugated planes of α-U are parallel to the shear plane (0 1 0). Therefore, the bonds that need to be reconstructed are located in the same corrugated planes. Finally, for type A STGBs, the shear plane is (0 0 1) while (0 1 0) is the tilt plane (or cut plane), and corrugated planes are perpendicular to the the shear plane. In order to generate a type A STGB, bonds oriented in the transverse direction of the

corrugation have to be reconstructed. It should be reiterated that type C STGBs have the highest average GB energy, followed by type A STGBs, with type B STGBs exhibiting the lowest grain boundary energies, which corresponds to a corrugated plane bonding conceptual framework. From this computational work, it is observed that both the degree and type of bond reconstruction along corrugated planes, in addition to the atomic misfit within the interface, are important to determine the GB energy of a STGB. By further analysis of GB structure using different methodologies can confirm the change of GB energy with misorintation angle, shear plane and temperature [44**?**].

3.1.2. Effect of temperature

To study the effect of temperature on GB energy of α-U STGBs, twenty-two STGBs (eight from type A, seven from type B, and seven from type C) are selected for further analysis. The studied temperatures are 300 K, 400 K, 500 K, and 600 K. The GB energy as a function of temperature for different orientations is presented in Figure 5. Data points are connected by straight lines to guide the eye. To evaluate the temperature sensitivity, the lowest studied temperature, 300 K, is considered as the reference point.

From Figure 5(a), in general, there is a decreasing trend of the GB energy of type A STGBs up to 400 K, followed by an increasing trend up to 600 K. The minimum grain boundary energy occurs for the ($\bar{1}$ $\bar{3}$ 12 0) plane at all temperatures (the arithmetic average of GB energy of this plane is 0.64 0.25 J/m^2 over the temperature range). However, the maximum energy STGB is not same for all temperatures studied. The maximum grain boundary energy occurs at the ($\bar{3}$ 2 0)$\langle$1 0 0$\rangle$ at 300 K and 400 K, but occurs at the ($\bar{3}$ 3 0)$\langle$1 0 0$\rangle$ and the ($\bar{3}$ 12 0)$\langle$1 0 0$\rangle$ at 500 K and 600 K, respectively. The ($\bar{1}$ $\bar{3}$ 12 0)$\langle$1 0 0$\rangle$ orientation is also one of the lowest energy type A STGBs , superseded only by special grain boundaries denoted by the cusps in Figure 3(a). The ($\bar{3}$ 12 0)$\langle$1 0 0$\rangle$ STGB shows the largest dependency on temperature, as its value varies by 3423.4% over the temperature range. The lowest temperature sensitivity is observed at the ($\bar{1}$ 12 0)$\langle$1 0 0$\rangle$ STGB, where the GB energy varies by 6.9% over the studied temperature range. The average change in GB energy over the studied temperature range is observed to be 15.814.5%, or 0.12 0.11 J/m^2.

Type B grain boundaries (Figure 5(b)) show a behavior similar to that of the type A grain boundaries. For nearly all of the studied planes the lowest energy is attained at 400 K, while the highest energy is observed at 600 K. The ($\bar{3}$ $\bar{2}$ 0 25) plane shows the largest dependency on temperature as its value varies by 18.3%. This plane also 1) plane has the lowest energy at every temperature (average over temperature range 0.59 J/m^2). The ($\bar{1}$ 0 15) plane displays a GB energy maximum of 0.71 J/m^2 at 300 K, however, the grain boundary energy of this plane also has the the least variation with temperature among those studied (3.3%). The ($\bar{1}$ 0 4)$\langle$0 0 1$\rangle$ STGB exhibits the highest GB energy at all studied temperatures, and the largest dependency on temperature as its value varies by 10.3%.. The average change in GB energy over the studied temperature range with respect to GB energy at 300 K is observed to be 7.86%, or 0.06 0.07 J/m^2.

For type C STGBs, the grain boundary energy shows an increasing trend with temperature, which accelerates with increasing temperature, see Figure 5(c). For example, the (0 72 $\overline{25}$)$\langle$0 0 1$\rangle$ STGB shows an increase of grain boundary energy from 300 K to 400 K of 4%, from 400 K to 500 K of 24.3%, and from 500 K

to 600 K of 39.4%. Among the grain boundary planes, the (0 18 $\overline{25}$) plane exhibits the lowest GB energy at each temperature studied (the average GB energy over the temperature range studied for this plane is 0.42 J/m^2). At both 300 K and 400 K, the maximum grain boundary energy is observed for the (0 36 $\overline{5}$) plane, while, at both 500 K and 600 K, the maximum grain boundary energy is observed for the (0 9 $\overline{10}$) plane. The (0 6 $\overline{5}$) plane has the least dependency on temperature as it varies by 0.44 J/m^2, or 45.9% from the GB energy at 300K. The lowest energy STGB (0 18 $\overline{25}$)$\langle$0 0 1$\rangle$ has the highest temperature dependence, as it increases by 176.8% from its value at 300 K. This (0 18 $\overline{25}$)$\langle$0 0 1$\rangle$ STGB is one of the lowest energy planes of STGB type C. The average change in GB energy over the studied temperature range is observed to be 82%, or 0.56 J/m^2. Compared to type A and B grain boundaries, type C is significantly more temperature sensitive.

The current work generally finds that for α-U STGBs, the GB energy is positively correlated with temperature (specifically from 400 K to 600 K). The temperature dependence of type C STGBs is similar to results for type A STGB of U_3Si_2 [41], and this trend is also observed in γ-U type A STGBs [41]. However, the GB energy of α-U STGBs is more temperature sensitive than UO_2, as the GB energy of UO_2 changes by only about 7% from 300 K to 600 K [45]. The current work indicates that at lower temperatures, there is less driving force for grain growth due to the lower grain boundary energy, as GB velocity is proportional to driving force and GB energy is prportional to GB energy [13]. This can lead to a relatively stable fine-grained microstructure, which can hinder dislocation movement and can lead to lower ductility within the material. Combined with a fine-grained microstructure, high stresses associated with twinning may not be relieved by slip, possibly reducing α-U ductility. Experimental evidence indicates that below 573 K, twinning activities of α-U increase with decreasing temperature, down to 198 K [17, 46, 47]. From the current work, GB energy of two probable twinning orientataions, ($\overline{3}$ 12 0)$\langle$1 0 0$\rangle$ and (0 18 $\overline{25}$)$\langle$0 0 1$\rangle$ has a positive relation with temperature 400 K to 600 K and 300 K to 600 K respectively. And both of them exhibits more temperature sensitivity with respect to room temperature than other general STGBs of their respective type (type A and C).

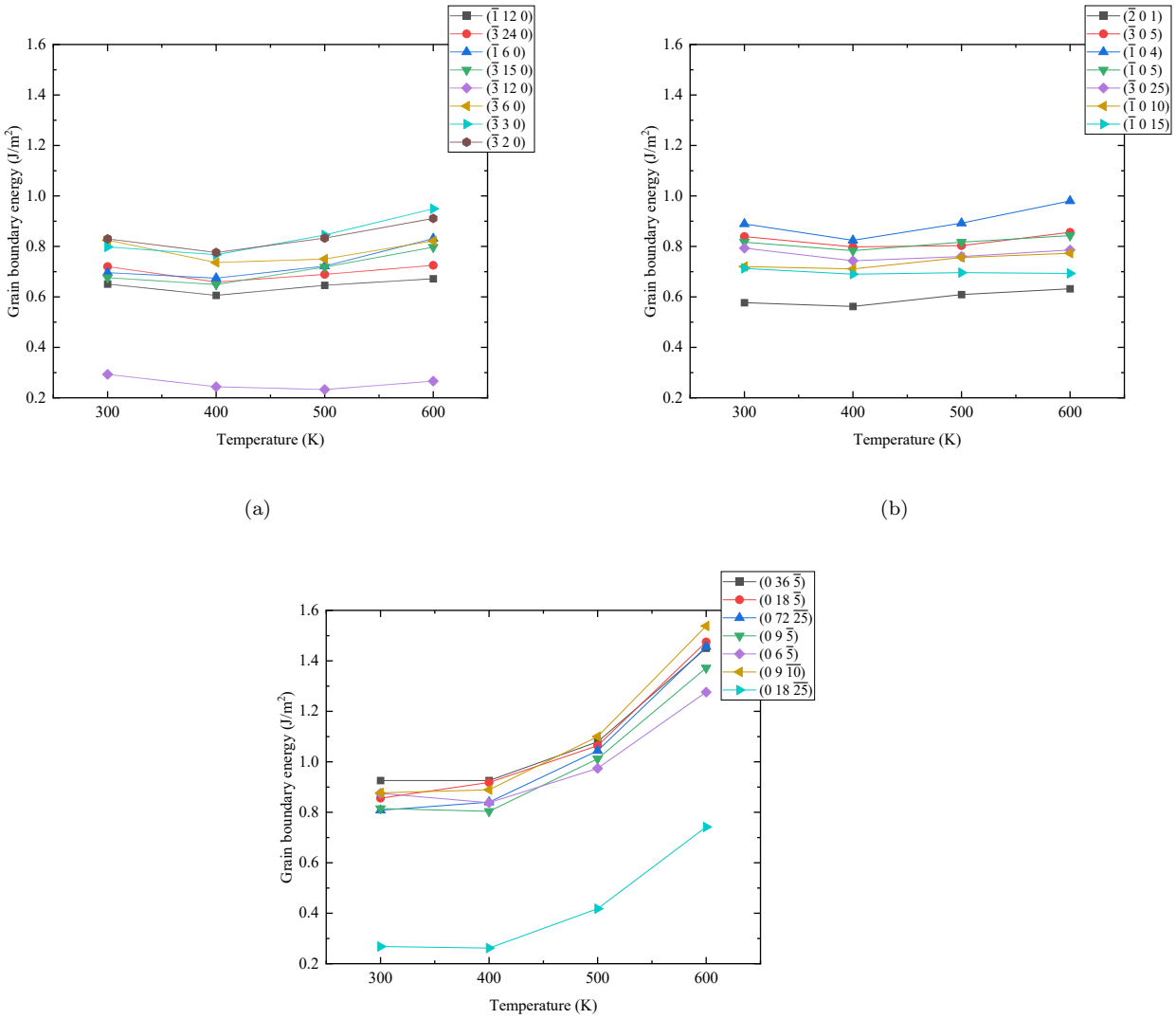

Figure 5: Grain boundary energy of selected STGBs of (a) type A, (b) type B, and (c) type C as a function of temperature

3.2. Surface Energies

3.2.1. Effect of tilt angle

In this section, the dependence of surface energy on tilt angle is discussed. The surfaces considered in this work are only those which are related to the STGBs. For instance, a STGB characterized by $(\overline{3}\ 6\ 0)\langle 1\ 0\ 0\rangle$ will be analyzed as a surface characterized by $(\overline{3}\ 6\ 0)$. The effect of tilt angle (surface orientation) on the surface energy of type A, type B, and type C surfaces is plotted in Figure 6. The surface energies of the (1 0 0), (0 1 0), and (0 0 1) planes have been also evaluated. The tilt angle of the studied surfaces ranges from 0° to 180° and the energies are characterized at 500 K.

Type A surfaces have an average surface energy of 1.25 J/m^2, with the ~~maximum surface energy observed for~~ minimum energy surface observed for both the $(\overline{3}\ 12\ 0)$ ~~plane (1.41 J/m^2), and the minimum energy surface observed for the~~ and $(\overline{3}\ \overline{12}\ 0)$ plane which are identical (1.0 J/m^2). Interestingly, ~~these two planes are perpendicular to each other, and~~ the $(\overline{3}\ \overline{12}\ 12\ 0)\langle 1\ 0\ 0\rangle$ STGB also has the lowest GB energy of type A. The maximum surface energy observed within a range of 1.35 J/m^2 to 1.38 J/m^2, whereas the surface energy of (0 1 0) is slightly higher than this limit (1.39 J/m^2). The shear plane for a type A STGB is (0 0 1) and this plane has 1-fold symmetry. Because of this, there is ~~no discernible trend in both~~ mirror symmetry in the surface energy plot as a function of tilt angle (Figure 6(a)) and the GB energy as a function of misorientation angle (Figure 3(a)) along the tilt axis $\langle 1\ 0\ 0\rangle$. The general trend of surface energy (from 0° to 90°) is to increase from small tilt angle 5° upto 15°, then decrease till 65° followed by an increase upto 90°.

~~Unlike~~ Like type A surfaces, a mirror symmetry with respect to tilt angle 90° is apparent in Figure 6(b) for type B surfaces, though a more simplified general trend is found, an increase upto 30 followed by a decrease till 90°. This occurs because of the 180° rotational symmetry with respect to the diagonal direction, [1 0 1] of the (0 1 0) plane, and the (0 1 0) is the shear plane of type B STGBs of the α-U unit cell. The highest energy surface is the $(\overline{9}\ 0\ 25)$ plane (identical to the $(\overline{9}\ 0\ \overline{25})$ plane), having a surface energy of 1.30 J/m^2. The lowest energy has been observed for the (0 0 1) plane with a surface energy of 1.11 J/m^2, and the second lowest energy surface is (1 0 0) with a value of 1.13 J/m^2. The (0 0 1) surface is the lowest energy surface among all type B surfaces. The average surface energy of type B was found to be 1.21 J/m^2. Among the three types of studied surfaces, type B has the least sensitivity to surface tilt angle and the lowest average surface energy.

Type C surface energies as a function of tilt angle at 500 K are shown in Figure 6(c). Due to the ~~absence of symmetry along the diagonal~~ 1- fold symmetry along of the (1 0 0) shear plane of the α-U unit cell, there is ~~no discernible pattern~~ mirror symmetry in the surface energy plot ~~,~~ excluding the thermal fluctuations. General trend of type C surfaces is a bit similar to that observed for type A surfaces~~. The maximum surface energy has been observed at the $(0\ \overline{18}\ \overline{25})$ plane with a surface energy of 1.52 J/m^2. This is the maximum energy surface among all eighty-three studied surfaces.~~ , a decrease upto 35°, then an increase till 65° followed by a decrease upto 90 °. However, there is ~~no~~ neither any statistically significant low energy nor any high energy surface that can be observed for type C surfaces. The lowest surface energy ranges between

1.10 J/m^2 and 1.11 J/m^2 for three surfaces, including the (0 $\overline{9}$ $\overline{10}$), (0 9 $\overline{10}$), and (0 0 1) planes. The highest surface energy exist among the (0 $\overline{72}$ $\overline{25}$), (0 72 $\overline{25}$), and (0 1 0) planes, ranging between 1.36 J/m^2 and 1.39 J/m^2. Similar to type C STGBs (Figure 3(c)), type C surfaces exhibit the highest average surface energy at 1.26 J/m^2.

Mirror symmetries that have been observed in all three types of surfaces matches with the crystallography of the corresponding shear planes. Type A, B and C surfaces have an average surface energy larger than their corresponding GB energy by 39.3%, 38%, and 22.7%, respectively. In a recent study, the surface energy of seven basic surfaces in α-U were calculated using density functional theory [34]. Among these surfaces, the (0 0 1) surface possesses the lowest energy, which agrees with the findings from the current work. However, the magnitude of the surface energy in this work does not directly correspond to the work in [34], where the (0 0 1) surface energy was characterized as 1.76 J/m^2, while our results indicate a surface energy of 1.11 J/m^2. However, the global arithmetic average of all surface energies calculated for the STGBs, in this work is 1.4 J/m^2, which falls within the range of available computational data on surface energy of α-U [31, 33, 34, 48]. Comparing to other fuel systems, the magnitude of the average surface energy of α-U (approximately 1.32 J/m^2) is higher than the γ-U [43] surface energy (1.15 J/m^2) at 600 K, while it is lower than the surface energy of U_3Si_2 [41] (approximately 1.78 J/m^2) at the same temperature. The surface energy of {1 0 0} planes in UO_2 have been observed to be between 1.69 J/m^2 and 1.92 J/m^2 (calculated utilizing MD [30]) at 300 K. This is higher than the (1 0 0), (0 1 0) and (0 0 1) surfaces of α-U at 500 K from this work, which is similar to the comparisons between the GB energies between the two materials.

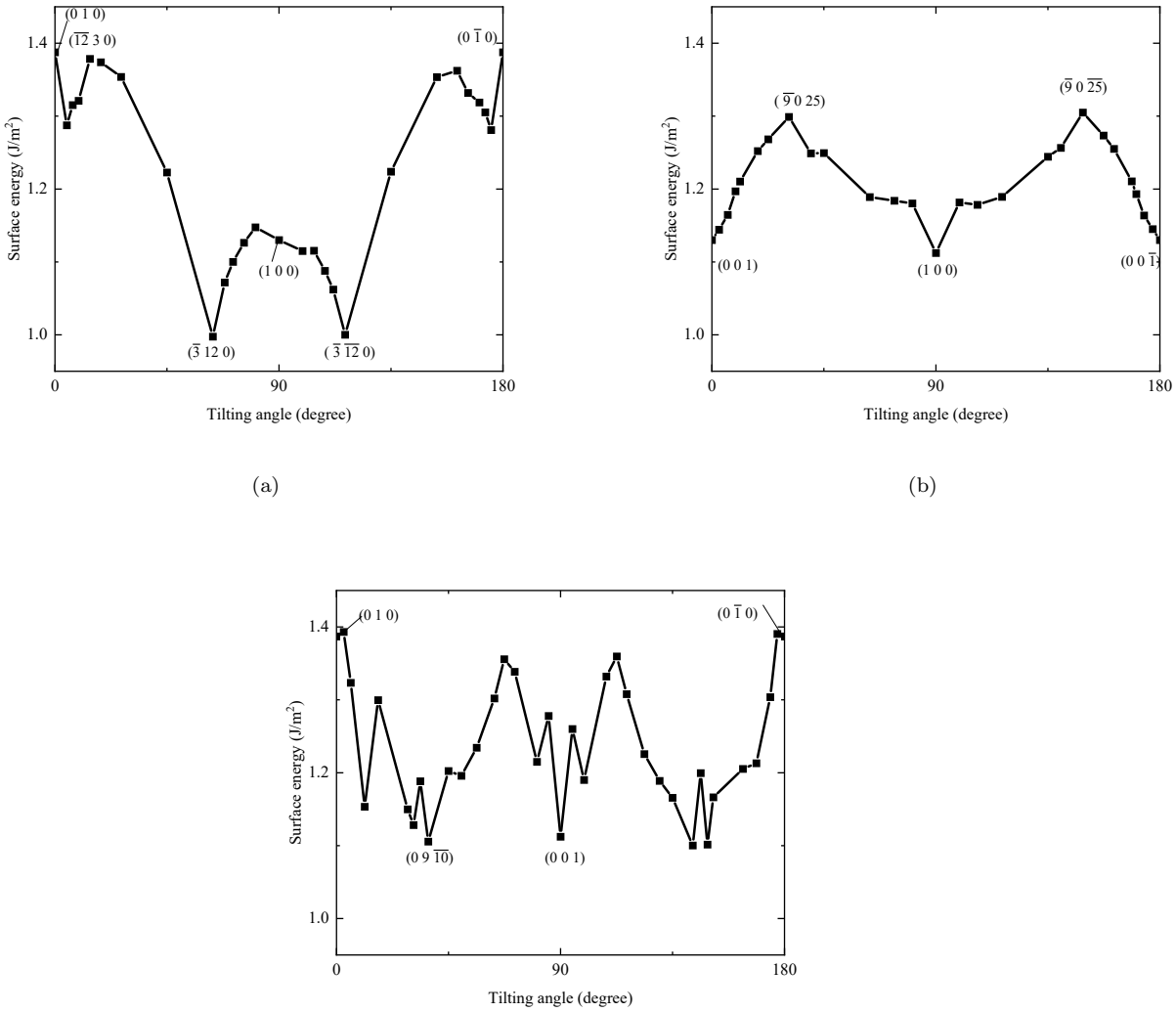

Figure 6: Surface energy of surfaces of (a) type A, (b) type B, and (c) type C as a function of tilt angle at 500 K.

3.2.2. Effect of temperature

An investigation of surface energy variation with temperature is performed, similar to the investigation of GB energy with temperature. In Figure 7, surface energies of type A, B, and C surfaces are displayed as a function of temperature. To study the effect of temperature on surface energy, a subset of eight planes have been chosen from type A, seven from type B, and seven from type C. All of these planes range between 0° and 90° misorientation angle.

From Figure 7(a), the common trend of temperature dependency of type A STGB surfaces is a decrease from 300 K to 400 K, followed by a linear increase up to 600 K. The rate of increase depends upon the surface orientation. The ($\bar{3}$ ~~15~~ 12 0) plane exhibits the lowest surface energy over the entire temperature range, and the ($\bar{3}$ ~~12~~ 2 0) plane exhibits the highest surface energy over nearly the entire temperature range. The surface planes ($\bar{3}$ ~~15~~ 12 0) and ($\bar{3}$ ~~12~~ 2 0) have a average surface energy of ~~1.09~~ 1.01 J/m^2 and ~~1.41~~ 1.37 J/m^2, respectively, over the temperature range investigated. The smallest dependency on temperature has been observed at the ($\bar{3}$ 12 0) surface plane (varying by a maximum of ~~2.6~~2.9% from its surface energy of ~~1.44~~ 1.02 J/m^2 at 300 K) and the greatest dependency at the ($\bar{3}$ 3 0) plane (varying by a maximum of 6% from its surface energy of 1.32 J/m^2 at 300 K).

Type B surfaces in Figure 7(b) typically display a slight decrease in the surface energy from 300 K to 400 K, followed by an increase in surface energy up to 600 K, though the variation with temperature is noticeably less than either type A or type C surfaces. The ($\bar{1}$ 0 15) plane consistently exhibits the lowest surface energy with an average value of 1.17 J/m^2, and the ($\bar{1}$ 0 4) plane has the highest surface energy with an average value of 1.27 J/m^2 over the temperature range. The average change in surface energy from 300 K to 600 K is observed to be 2.5% for this subset of surfaces. The most temperature sensitive surface is the ($\bar{1}$ 0 5) plane, showing an increase of 4.2%, while the least temperature sensitive surface is the ($\bar{1}$ 0 10) plane, which varies by 1.6% from its surface energy value attained at 300 K.

All the studied surfaces of type C exhibit the highest surface energy at 600 K. The (0 9 $\bar{5}$), (0 6 $\bar{5}$), and (0 9 $\overline{10}$) planes have their lowest surface energy at 400 K, though, their energy is lower by only 0.01 J/m^2 from the respective value at 300 K. The rest of the surface planes studied attain a minimum energy at 300 K. Therefore, it can be said that type C surfaces have a trend of increasing surface energy with increasing temperature 7(c). This trend is similar to that observed in the type C STGBs, but the rate of increase is slower than that of the corresponding type C STGBs. For example, the (0 72 $\overline{25}$) plane shows an increase of surface energy from 300 K to 400 K of 1.1%, from 400 K to 500 K of 7.2%, and from 500 K to 600 K of 12.8%, see Figure 7(c), and corresponding values of (0 72 $\overline{25}$)⟨0 0 1⟩ STGB energy are 4%, 24.3%, and 39.4%, see Figure 5(c). The (0 18 $\overline{25}$) surface displays the lowest surface energy over the entire temperature range with an average value of 1.13 J/m^2, and the (0 72 $\overline{25}$) plane displays the highest surface energy among all the studied seven planes with an average value of 1.35 J/m^2. The (0 6 $\bar{5}$) plane has the least sensitivity to temperature, as it varies by only 1.2% over the temperature range with respect to surface energy at 300 K . In the similar fashion, the (0 72 $\overline{25}$) plane varies by 22.2% over the temperature range. Comparing with

the other two types of surfaces, type C surfaces are significantly more sensitive to temperature.

When considering the average variation in surface energy with temperature, type C STGBs in α-U have a similar trend to γ-U surfaces [43]. However, the trend of surface energy for type A and B surfaces in α-U is more similar to U_3Si_2 surface energies [41]. The surface energy change from 300 K to 600 K for type A and B STGBs shows that they possess a smaller temperature dependency than UO_2, which was observed to be 7.4% [45], whereas type C shows a stronger dependency on temperature.

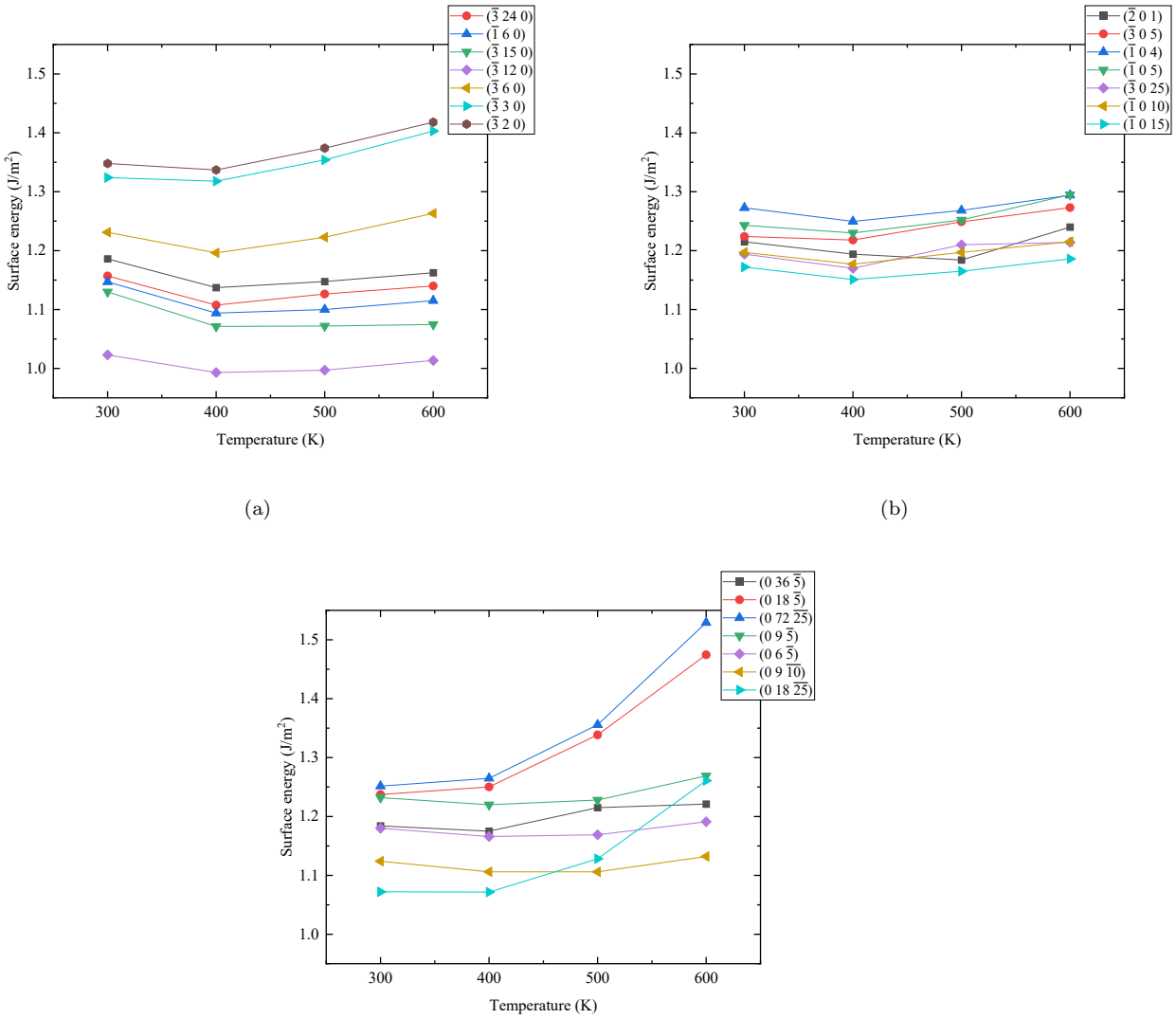

Figure 7: Surface energy of selected surfaces of (a) type A, (b) type B, and (c) type C as a function of temperature.

3.3. Work of adhesion for α-U

3.3.1. Effect of misorientation angle

The work of adhesion (WAd) of different STGBs at 500 K is calculated via Equation 2 and plotted as a function of the corresponding misorientation angle in Figure 8. The WAd is defined here as the energy required to form two surfaces from a given STGB 2. A lower value for the work of adhesion represents less total energy required to break apart a GB into two separate free surfaces. Thus, orientations with low WAd are potential sites for cleavage or fracture, or the nucleation of the α tearing phenomenon [26].

Before explaining Figure 8, it should be emphasized that in all types of STGBs, the (1 0 0) and the (0 0 1) planes represent the pure crystalline system, with no true GB present. Thus, the WAd values for the (1 0 0) and (0 0 1) planes (2.26 J/m^2 and 2.22 J/m^2, respectively) are actually the WAd values of the perfect crystal system, which is simply two times the surface energy of the (1 0 0) or (0 0 1) plane. Conversely, grain boundaries are observed at the (0 1 0) misorientation plane because of the absence of mirror symmetry with respect to this plane. This is why, for misorientation angle 0° or 360° in type A and C STGBs, GBs are formed .

The maximum WAd of type A STGBs has been found for the (0 1 0) STGB and the minimum for the ($\overline{3}$ 15 0) STGB, with magnitudes of 2.4 J/m^2 and 1.43 J/m^2, respectively, as seen in Figure 8(a). In order to split a STGB of type A into two type A surfaces, on average of ~~1.8~~ 1.78 J/m^2 of energy is required. For type B orientations, no statistically significant minimum or maximum is observed, as all the WAd values reside from 1.6~~-1.8~~ - 1.8 J/m^2 (see Figure 8(b)). Type C STGBs exhibit the lowest average WAd from the three plane types, whereas type C STGBs and surfaces exhibit the highest GB and surface energies. The highest WAd is found for the (0 1 0) plane (2.41 J/m^2), while the lowest WAd is observed for the (0 9 $\overline{10}$) ~~and (~~ plane (similar to (0 $\overline{9}$ $\overline{10}$) ~~planes~~plane), at 1.11 J/m^2 ~~and 1.16 J/m^2, respectively~~ (Figure 8(c)).

The WAd for type B STGBs is less sensitive to misorientation angle, as WAd values fluctuate within a very small range (1.6-1.8 J/m^2) compared to type A and C STGBs. Type B STGBs have an average WAd of ~~1.68~~ 1.75 J/m^2, while type A STGBs have an average WAd of ~~1.77~~ 1.78 J/m^2, and type C STGBs an average of ~~1.59~~ 1.61 J/m^2. ~~From Figure 8(a), type A STGBs have less strength to resist tearing when the misorientation planeis located more closely to the ⟨0 1 0⟩ direction. No such patterns are observed for type C STGBs~~ Aside from the mirror symmetry with tilt plane, there are no distinguishable pattern in WAd profile of the studied STGBs of α-U has observed.

Two possible twins in α-U found from the current study are the ($\overline{3}$ ~~$\overline{12}$~~ 12 0)⟨1 0 0⟩ STGB and the (0 18 $\overline{25}$)⟨0 0 1⟩ STGB. Although these STGBs are found to have very low energies, their WAd values are not significantly higher or lower than the average WAd of the respective type of STGB . The WAd of these STGBs are ~~1.7~~ 1.76 J/m^2 and 1.83 J/m^2, respectively. Among all the studied STGBs, ($\overline{3}$ ~~12~~ 2 0)⟨1 0 0⟩ has the maximum resistance to tearing (except the (1 0 0), (0 0 1), and (0 1 0) misorientation planes) ~~misorientation plane)~~ with a WAd of ~~2.0~~ 1.92 J/m^2, whereas the most susceptible orientation for tearing is the (0 9 $\overline{10}$)⟨0 0 1⟩ STGB, with a WAd of 1.11 J/m^2. GB energy of this orientation is also 1.11 J/m^2.

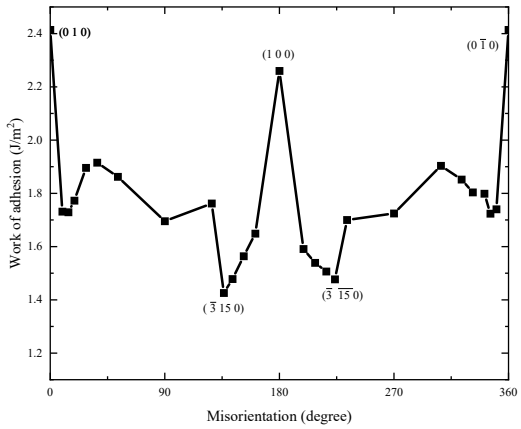

(a)

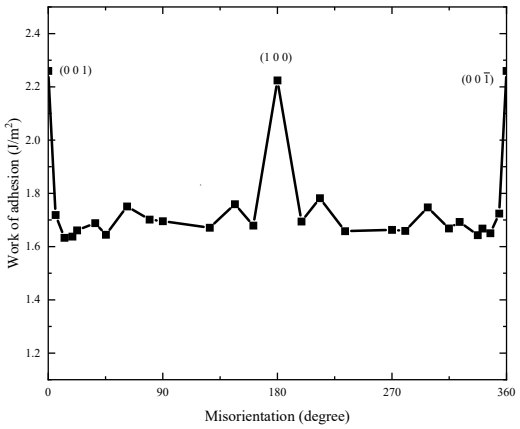

(b)

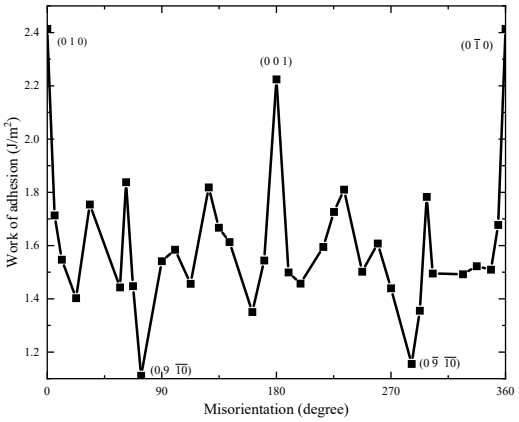

(c)

Figure 8: Work of Adhesion of STGBs of (a) type A, (b) type B, and (c) type C as a function of misorientation angle at 500 K.

Difference in misorientation angle between probable twinning orientation of type A STGB, $(\bar{3}\ 12\ 0)\langle 1\ 0\ 0\rangle$, and probable tearing site, $(\bar{3}\ 15\ 0)\langle 1\ 0\ 0\rangle$, is approximately 10°. Like type A STGBs, probable twinning site of type C STGBs ($(0\ 18\ \overline{25})\langle 0\ 0\ 1\rangle$) resided within 10° misorientation angle of probable twinning site ($(0\ 9\ \overline{10})\langle 0\ 0\ 1\rangle$).

The α-U WAd values can be compared with available literature on the WAd of other fuel systems. At 300 K, the WAd of UO_2 [30] GBs has a wide range, from 0.3 J/m^2 to 2.5 J/m^2. The work presented here demonstrates an approximate average WAd of 1.91 J/m^2 at 300 K, suggesting that the WAd of α-U STGBs is likely to be within the upper range of UO_2. α-U has a lower average WAd (approximately ~~1.71~~ 1.68 J/m^2) than γ-U (approximately 1.9 J/m^2) and U_3Si_2 (approximately 2.6 J/m^2) [43, 41] at 600 K. Hence, α-U is more prone to cleavage formation along GBs compared to other uranium based nuclear fuel.

3.3.2. Effect of temperature

Similar to GB energy and surface energy, the effect of temperature on WAd of α-U is investigated. For this analysis, twenty-two STGBs (eight from type A, seven from type B, and seven from type C) are selected for further analysis. The studied temperatures are 300 K, 400 K, 500 K, and 600 K; among them, 300 K is considered as the reference point to evaluate the temperature sensitivity. The WAd as a function of temperature for different STGBs is presented in Figure 9.

From Figure 9(a), it is observed that, unlike GB energy and surface energy of type A STGBs, WAd has an inverse relationship with temperature when the misorientation angle is greater than 90° (see Appendix Table 1 for associated misorientation angles). The least temperature sensitive (only 1%) STGB of type A is the $(\bar{3}\ 3\ 0)\langle 1\ 0\ 0\rangle$. However, the WAd changes by a maximum of ~~15.1~~14.7% for the $(\bar{3}$ ~~12~~ 15 $0)\langle 1\ 0\ 0\rangle$ STGB, which has the ~~maximum surface energy at 500 K (see Figure 6(a)) and the second highest~~ lowest WAd among all studied type A STGBs, with an average WAd of ~~2.0~~ 1.46 J/m^2 over the temperature range. The ~~lowest~~ highest WAd among the studied subset of type A STGBs is observed at the $(\bar{3}$ ~~15~~ 2 $0)$ plane, with an average WAd of ~~1.46~~ 1.9 J/m^2 across all temperatures. Moreover, this plane also hold the highest surface energy at all temperature. For a misorientation angle less than or equal to 90°, the increase in the WAd with temperature is not significant (maximum by 4.1% for STGB $(\bar{3}\ 6\ 0)\langle 1\ 0\ 0\rangle$). ~~The least temperature sensitive (only 1%) STGB of type A is the $(\bar{3}\ 3\ 0)\langle 1\ 0\ 0\rangle$.~~

Similar to both type B STGBs and surfaces (see Figure 7(b)), WAd shows only minimal variance (maximum of ~~5.1~~5.3%) with temperature, see Figure 9(b). The maximum variation is observed for the $(\bar{3}\ 0\ 5)\langle 0\ 0\ 1\rangle$ STGB, which shows an increase with temperature, but this increasing trend is not consistent for other planes, where some planes instead show a decrease in WAd with increasing temperature. The least sensitivity is found for the $(\bar{1}\ 0\ 10)$ plane, which is 2.1%. Among the seven type B STGBs studied, the range of WAd values decreases with temperature. For instance, at 300 K WAd has a range (maximum minus minimum) of 0.21 J/m^2, which is reduced with increasing temperature until it becomes 0.14 J/m^2 at 600 K. From this evidence, we can say that the dependence of WAd on misorientation angle is stronger at lower temperatures for type B STGBs, similar to type A and C.

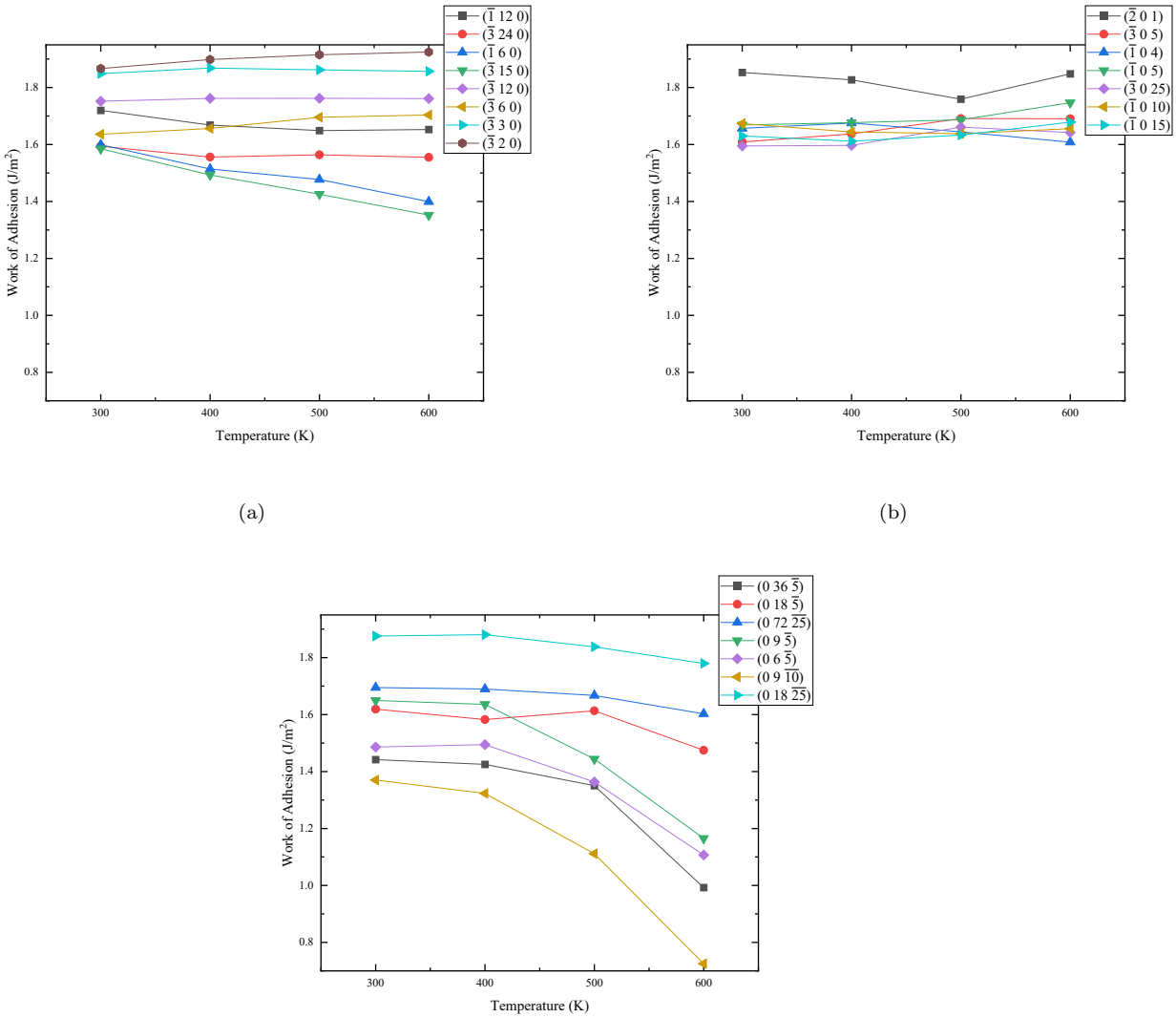

Figure 9: Work of Adhesion of selected STGBs of (a) type A, (b) type B, and (c) type C as a function of temperature.

The general trend of the WAd of type C STGBs is to decrease with temperature, as seen in Figure 9(c). The $(0\ 9\ \overline{10})\langle 0\ 0\ 1\rangle$ STGB shows the highest percentage (47%) decrease of WAd with respect to corresponding WAd at 300 K and also has the lowest WAd among the type C STGBs, see Figure 8(c), with an average WAd over the temperature range of 1.13 J/m^2. The least temperature sensitivity (5.1%) is observed for the $(0\ 18\ \overline{25})\langle 0\ 0\ 1\rangle$ STGB, which is one of the preferred twinning orientations. At all the studied temperatures, the $(0\ 18\ \overline{25})$ plane shows the highest WAd value (average WAd is 1.84 J/m^2) while the GB energy for this orientation is the lowest for all temperatures, see Figure 5(c).

We recall from Fig. 5 and 7 that the grain boundary energy (type A 14.5%, type B 6.6% and type C 82.2%) increases with temperature at a higher rate than the surface energy (type A 4.4%, type B 2.6% and type C 10.2%). Given this relationship and equation 2, the general trend of WAd is to decrease with temperature. This indicates that in general it is expected to require slightly less work to create two surfaces from a STGB as the temperature increases, which means α tearing is more favorable at higher temperature. This finding is also consistent with the literature [27, 49]. During irradiation, the anisotropic irradiation growth of individual grains in polycrystalline α-U generates stress concentrations at grain boundaries [50]. Additionally, anisotropic thermal expansion can generate additional internal stresses [51]. Due to these stress concentrations, micro-tearing may take place at the grain boundaries, generating void space and swelling [49]. At temperatures below about 623 K, polycrystalline α-U deforms plastically without the loss of density, but at temperatures of approximately 623 K to 723 K, a deformed microstructure with ragged cavities (indicative of grain boundary tearing) occurs. This behavior is specific to irradiated α-U, though similar behavior is evident during thermal cycling [27].

4. Conclusions

In this study, the grain boundary energy, surface energy, and work of adhesion of symmetric tilt grain boundaries in α-U have been calculated as a function of temperature and misorientation angle. Three types of STGBs (A, B, and C) are considered, which have a shear plane on either the (0 0 1), (0 1 0) or (1 0 0) planes, and corresponding tilt axes of $\langle 1\ 0\ 0\rangle$, $\langle 0\ 0\ 1\rangle$, and $\langle 0\ 0\ 1\rangle$, respectively. Due to the orthorhombic structure of α-U, the grain boundary energy, surface energy, and work of adhesion of all three types of interface properties not only depend on the misorientation angle, but also on the interface orientation. Two of the lowest grain boundary energies are found at the $(\overline{3}$ ~~$\overline{12}$~~ $\overline{12}\ 0)\langle 1\ 0\ 0\rangle$ and $(0$ ~~$\overline{18}$~~ $\overline{18}\ \overline{25})\langle 0\ 0\ 1\rangle$ orientations. These two STGBs can potentially form twins, as they have a very low GB energy. It is found that the $(0\ 9\ \overline{10})\langle 0\ 0\ 1\rangle$ STGB has the lowest work of adhesion, which indicates that it is the most probable site for grain boundary tearing among the studied STGBs. When STGBs have a (1 0 0) shear plane, a $\langle 0\ 0\ 1\rangle$ tilt axis, and a (0 1 0) tilt plane (type C), they typically have a higher energy compared to the other two types (A and B) of STGBs studied. However, if the STGB has a (0 0 1) shear plane, a $\langle 1\ 0\ 0\rangle$ tilt axis, and a (0 1 0) tilt plane (type A), then these orientations have more resistance to tearing (higher WAd). There is no consistent correlation as a function of misorientation angle for GB energy, surface energy, or WAd. At 500

K, the global arithmetic average of the surface energy (~~1.24~~ 1.23 J/m^2) is approximately 1.5 times the GB energy (~~0.82~~ 0.79 J/m^2), and the WAd is approximately twice the GB energy (~~1.67~~ 1.68 J/m^2). From the current analysis it is ascertained that as the temperature increases, both the GB and surface energy tend to increase, with the GB energy increasing more rapidly, leading to a decrease in the WAd with temperature. With respect to room temperature (300 K), values at 600 K have changed by an average of ~~34.4~~34.2% for GB energy, ~~5.5~~5.7% for surface energy, and ~~10.7~~10.1% for the WAd.

This study has provided the most comprehensive analysis of GBs and surfaces in α-U to date, illuminating the dependence of interfacial properties on crystallographic orientations and temperature, in addition to providing key geometrically averaged interfacial energy values. The information from this work will be utilized to study grain boundary evolution in polycrystalline α-U and deformation under irradiation, leading to the development of improved fuel performance models via physics-based mesoscale models.

5. Acknowledgement

Work supported through the INL Laboratory Directed Research and Development (LDRD) Program under DOE Idaho Operations Office Contract DE-AC07-05ID14517. This manuscript has been authored by Battelle Energy Alliance, LLC with the U.S. Department of Energy. The publisher, by accepting the article for publication, acknowledges that the U.S. Government retains a nonexclusive, paid-up, irrevocable, worldwide license to publish or reproduce the published form of this manuscript, or allow others to do so, for U.S. Government purposes. This research made use of the resources of the High Performance Computing Center at Idaho National Laboratory, which is supported by the Office of Nuclear Energy of the U.S. Department of Energy and the Nuclear Science User Facilities.

References

[1] W. Carmack, D. Porter, Y. Chang, S. Hayes, M. Meyer, D. Burkes, C. Lee, T. Mizuno, F. Delage, J. Somers, Metallic fuels for advanced reactors, Journal of Nuclear Materials 392 (2) (2009) 139 – 150, nuclear Fuels and Structural Materials 2. doi:https://doi.org/10.1016/j.jnucmat.2009.03.007.
URL http://www.sciencedirect.com/science/article/pii/S0022311509004103

[2] G. L. Hofman, Metallic Fuels, American Cancer Society, 2015, pp. 1–53. arXiv:https://onlinelibrary.wiley.com/doi/pdf/10.1002/9783527603978.mst0105.pub2, doi:10.1002/9783527603978.mst0105.pub2.
URL https://onlinelibrary.wiley.com/doi/abs/10.1002/9783527603978.mst0105.pub2

[3] G. Hofman, S. Hayes, M. Petri, Temperature gradient driving constituent redistribution in u-zr alloys, J. Nucl. Mater. 227 (1996) 277.

[4] B. Beeler, C. Deo, M. Baskes, M. Okuniewski, First principles calculations of the structure and elastic constants of α, β and γ uranium, Journal of Nuclear Materials 433 (1) (2013) 143 – 151. doi:https://doi.org/10.1016/j.jnucmat.2012.09.019.
URL http://www.sciencedirect.com/science/article/pii/S0022311512004965

[5] N. Stojić, J. Davenport, M. Komelj, J. Glimm, Prediction of a surface magnetic moment in alpha-uranium (03 2003).

[6] E. Y. Chen, C. Deo, R. Dingreville, Atomistic simulations of temperature and direction dependent threshold displacement energies in α- and γ-uranium, Computational Materials Science 157 (2019) 75 – 86. doi:https://doi.org/10.1016/j.commatsci.2018.10.026.
URL http://www.sciencedirect.com/science/article/pii/S0927025618306967

[7] F. C. FRANK, A note on twinning in alpha-uranium, Acta Metallurgica 1 (1953) 71 – 74.

[8] R. W. Cahn, Twinning and slip in α uranium, Acta Crystal 4 (1951) 470.

[9] L. T. LLOYD, C. S. BARRETT, Thermal expansion of alpha uranium, Journal of Nuclear Materials 18 (1966) 55 – 59.

[10] E. S. FISHER, Temperature dependence of the elastic moduli in alpha uranium single crystals, part iv (298 k to 923 k), Journal of Nuclear Materials 18 (1966) 39 – 54.

[11] B. A. Loomis, T. H. Blewitt, A. C. Klank, S. B. Gerber, Elongation of uranium single crystals during neutron irradiation, Applied Physics Letters 5 (7) (1964) 135–137. arXiv:https://doi.org/10.1063/1.1754086, doi:10.1063/1.1754086.
URL https://doi.org/10.1063/1.1754086

[12] T. J. Barrett, R. J. McCabe, D. W. Brown, B. Clausen, S. C. Vogel, M. Knezevic, Predicting deformation behavior of α-uranium during tension, compression, load reversal, rolling, and sheet forming using elasto-plastic, multi-level crystal plasticity coupled with finite elements, Journal of the Mechanics and Physics of Solids 138 (2020) 103924. doi:https://doi.org/10.1016/j.jmps.2020.103924.
URL http://www.sciencedirect.com/science/article/pii/S0022509620301605

[13] G. Gottstein, L. S. Shvindlerman, Grain boundary migrations in metals: thermodynamics, kinetics, applications, CRC Press, 2010.

[14] D. A. Carpenter, J. L. Pugh, D. F. Teter, Control of grain boundaries in orthorhombic alpha-uranium, Microscopy and Microanalysis 11 (S02) (2005) 1792–1793. doi:10.1017/S1431927605506640.

[15] B. A. Bilby, A. G. Crocker, The theory of the crystallography of deformation twinning, Proceedings of the Royal Society of London. Series A, Mathematical and Physical Sciences 288 (1413) (1965) 240–255.
URL http://www.jstor.org/stable/2415026

[16] M. Steiner, R. McCabe, E. Garlea, S. Agnew, Monte carlo modeling of recrystallization processes in α-uranium, Journal of Nuclear Materials 492 (2017) 74 – 87. doi:https://doi.org/10.1016/j.jnucmat.2017.04.026.
URL http://www.sciencedirect.com/science/article/pii/S0022311516310212

[17] M. Knezevic, R. J. McCabe, C. N. Tomé, R. A. Lebensohn, S. R. Chen, C. M. Cady, G. T. Gray III, B. Mihaila, Modeling mechanical response and texture evolution of α-uranium as a function of strain rate and temperature using polycrystal plasticity, International Journal of Plasticity 43 (2013) 70 – 84. doi:https://doi.org/10.1016/j.ijplas.2012.10.011.
URL http://www.sciencedirect.com/science/article/pii/S0749641912001647

[18] R. W. Cahn, Plastic deformation of α uranium ;twinning and slip, Acta Metallurgica 1 (1953) 49 – 70.

[19] R. O. TEEG, R. E. OGILVIE, Effect of orientation and temperature on the modes of deformation of uranium, Journal of Nuclear Materials 3, No. 1 (1961) 81 – 88.

[20] A. G. CROCKER, The crystallography of reformation thinning in alpha-uranium, Journal of Nuclear Materials 16 (1965) 306 – 326.

[21] R. Field, R. McCabe, D. Alexander, D. Teter, Deformation twinning and twinning related fracture in coarse-grained α-uranium, Journal of Nuclear Materials 392 (1) (2009) 105 – 113. doi:https://doi.org/10.1016/j.jnucmat.2009.03.054.
URL http://www.sciencedirect.com/science/article/pii/S0022311509004735

[22] R. McCabe, L. Capolungo, P. Marshall, C. Cady, C. Tomé, Deformation of wrought uranium: Experiments and modeling, Acta Materialia 58 (16) (2010) 5447 – 5459. doi:https://doi.org/10.1016/j.actamat.2010.06.021.
URL http://www.sciencedirect.com/science/article/pii/S1359645410003757

[23] C. Calhoun, J. Wollmershauser, D. Brown, R. Mulay, E. Garlea, S. Agnew, Thermal residual strains in depleted α-u, Scripta Materialia 69 (8) (2013) 566 – 569. doi:https://doi.org/10.1016/j.scriptamat.2013.06.004.
URL http://www.sciencedirect.com/science/article/pii/S1359646213003060

[24] R. McCabe, R. Field, D. Brown, D. Alexander, C. Cady, Electron backscatter diffraction (ebsd) characterization of twinning related deformation and fracture in α-uranium, Microscopy and Microanalysis 14 (S2) (2008) 638–639. doi:10.1017/S1431927608083554.

[25] P. Zhou, D. Xiao, W. Wang, G. Sang, Y. Zhao, D. Zou, L. He, Twinning behavior of polycrystalline alpha-uranium under quasi static compression, Journal of Nuclear Materials 478 (2016) 83 – 90. doi:https://doi.org/10.1016/j.jnucmat.2016.05.041.
URL http://www.sciencedirect.com/science/article/pii/S002231151630246X

[26] J. Rest, Kinetics of fission-gas-bubble-nucleated void swelling of the alpha-uranium phase of irradiated u-zr and u-pu-zr fuel, Journal of Nuclear Materials 207 (1993) 192 – 204. doi:https://doi.org/10.1016/0022-3115(93)90261-V.
URL http://www.sciencedirect.com/science/article/pii/002231159390261V

[27] C. L. ANGERMAN, J. G. R. CASKEY, Swelling of uranium by mechanical cavitation, Journal of Nuclear Materials 13, No. 2 (1964) 182 – 196.

[28] R. McCabe, A. Richards, D. Coughlin, K. Clarke, I. Beyerlein, M. Knezevic, Microstructure effects on the recrystallization of low-symmetry alpha-uranium, Journal of Nuclear Materials 465 (2015) 189 – 195. doi:https://doi.org/10.1016/j.jnucmat.2015.04.055.
URL http://www.sciencedirect.com/science/article/pii/S0022311515002743

[29] G. S. Rohrer, Grain boundary energy anisotropy: a review, Journal of Materials Science 46 (2011) 5881 – 5895. doi:https://doi.org/10.1007/s10853-011-5677-3.
URL https://doi.org/10.1007/s10853-011-5677-3

[30] E. Bourasseau, A. Mouret, P. Fantou, X. Iltis, R. Belin, Experimental and simulation study of grain boundaries in uo2, Journal of Nuclear Materials 517 (02 2019). doi:10.1016/j.jnucmat.2019.02.033.

[31] J. E. BAINBRIDGE, B. HIJDSON, On the techniques for observing fission gas bubbles in uranium, Journal of Nuclear Materials 17 (1965) 237 – 244.

[32] J. Kollár, L. Vitos, H. L. Skriver, Surface energy and work function of the light actinides, Phys. Rev. B 49 (1994) 11288–11292. doi:10.1103/PhysRevB.49.11288.
URL https://link.aps.org/doi/10.1103/PhysRevB.49.11288

[33] C. D. Taylor, Evaluation of first-principles techniques for obtaining materials parameters of α-uranium and the (001) α-uranium surface, Phys. Rev. B 77 (2008) 094119. doi:10.1103/PhysRevB.77.094119.
URL https://link.aps.org/doi/10.1103/PhysRevB.77.094119

[34] S.-Q. Huang, X.-H. Ju, First-principles study of properties of alpha uranium crystal and seven alpha uranium surfaces, Journal of Chemistry 2017 (2017). doi:https://doi.org/10.1155/2017/8618340.

[35] D. Wolf, Structure-energy correlation for grain boundaries in f.c.c. metals—iii. symmetrical tilt boundaries, Acta Metallurgica et Materialia 38 (5) (1990) 781 – 790. doi:https://doi.org/10.1016/0956-7151(90)90030-K.
URL http://www.sciencedirect.com/science/article/pii/095671519090030K

[36] S. Plimpton, Fast parallel algorithms for short-range molecular dynamics, J. Comp. Phys. 117 (1995) 1–19.

[37] A. Stukowski, Visualization and analysis of atomis simulation data with ovito - the open visulaization tool, Modeling and Simulation of Materials Science and Engineering 18 (2010) 015012.

[38] T. Frolov, W. Setyawan, R. J. Kurtz, J. Marian, A. R. Oganov, R. E. Rudd, Q. Zhu, Grain boundary phases in bcc metals, Nanoscale 10 (2018) 8253–8268. doi:10.1039/C8NR00271A.
URL http://dx.doi.org/10.1039/C8NR00271A

[39] D. Smirnova, A. Kuksin, S. Starikov, V. Stegailov, Atomistic modeling of the self-diffusion in gamma u and gamma u-mo, Phys. Met. and Metall. 116 (2015) 445.

[40] S. Starikov, L. Kolotova, A. Kuksin, D. Smirnova, V. Tseplyaev, Atomistic simulation of cubic and tetragonal phases of u-mo alloy: Structure and thermodynamic properties, Journal of Nuclear Materials 499 (2018) 451 – 463. doi:https://doi.org/10.1016/j.jnucmat.2017.11.047.
URL http://www.sciencedirect.com/science/article/pii/S0022311517312229

[41] B. Beeler, M. Baskes, D. Andersson, M. W. Cooper, Y. Zhang, Molecular dynamics investigation of grain boundaries and surfaces in u3si2, Journal of Nuclear Materials 514 (2019) 290 – 298. doi:https://doi.org/10.1016/j.jnucmat.2018.12.008.
URL http://www.sciencedirect.com/science/article/pii/S0022311518312285

[42] J. Stobo, C. Robinson, G. May, W. Blackburn, Preferred orientations in alpha uranium, Acta Metallurgica 13 (6) (1965) 629 – 634. doi:https://doi.org/10.1016/0001-6160(65)90125-2.
URL http://www.sciencedirect.com/science/article/pii/0001616065901252

[43] B. Beeler, Y. Zhang, Y. Gao, An atomistic study of grain boundaries and surfaces in /*gamma*u-mo, Journal of Nuclear Materials 507 (2018) 248 – 257. doi:https://doi.org/10.1016/j.jnucmat.2018.05.007.
URL http://www.sciencedirect.com/science/article/pii/S0022311518301454

[44] Q. Zhu, A. Samanta, B. Li, R. E. Rudd, T. Frolov, Predicting phase behavior of grain boundaries with evolutionary search and machine learning, Nature Communications (02 2018).

[45] P. Nikolopoulos, S. Nazaré, F. Thümmler, Surface, grain boundary and interfacial energies in uo2 and uo2-ni, ournal of Nuclear Materials 71 (1) (1977) 89 – 94. doi:https://doi.org/10.1016/0022-3115(77)90191-X.
URL http://www.sciencedirect.com/science/article/pii/002231157790191X

[46] D. Brown, M. Bourke, B. Clausen, D. Korzekwa, R. Korzekwa, R. McCabe, T. Sisneros, D. Teter, Temperature and direction dependence of internal strain and texture evolution during deformation of uranium, Materials Science and Engineering: A 512 (1) (2009) 67 – 75. doi:https://doi.org/10.1016/j.msea.2009.02.004.
URL http://www.sciencedirect.com/science/article/pii/S0921509309001452

[47] D. M. R. TAPLIN, J. W. MARTIN, The effect of grain size and cold work on the tensile properties of alpha-uranium, Journal of the Less- common Metals 7 (1964) 89 – 97.

[48] C. D. Taylor, Erratum: Evaluation of first-principles techniques for obtaining materials parameters of α-uranium and the (001) α-uranium surface [phys. rev. b 77, 094119 (2008)], Phys. Rev. B 80 (2009) 149906. doi:10.1103/PhysRevB.80.149906.
URL https://link.aps.org/doi/10.1103/PhysRevB.80.149906

[49] T. K. B. R. D. Leggett, B. Mastel, Irradiation behaviour of high purity uranium, hanford Laboratories, HW- 79559 (November 1963).

[50] A. Jokisaari, Irradiation-induced internal stresses in polycrystalline α-uranium: a mesoscale mechanical approach, Computational Materials Science 176 (2020) 109545. doi:https://doi.org/10.1016/j.commatsci.2020.109545.
URL http://www.sciencedirect.com/science/article/pii/S0927025620300367

[51] A. A. Rezwan, A. M. Jokisaari, M. R. Tonks, Modeling brittle fracture due to anisotropic thermal expansion in polycrystalline materials (2020).

6. Appendix

Table 1: Studied STGBs of α-U.

type A		type B		type C	
tilting axis	$\langle 1\ 0\ 0\rangle$	tilting axis	$\langle 0\ 0\ 1\rangle$	tilting axis	$\langle 0\ 0\ 1\rangle$
tilt plane or cut plane	(0 1 0)	tilt plane or cut plane	(1 0 0)	tilt plane or cut plane	(0 1 0)
shear plane	(0 0 1)	shear plane	(0 1 0)	shear plane	(1 0 0)
misorientation angle (deg)	STGB plane	misorientation angle (deg)	STGB plane	misorientation angle (deg)	STGB plane
9.53	$(\overline{6}\ 1\ 0)$	5.72	$(\overline{3}\ 0\ 100)$	5.72	$(0\ 3\ \overline{50})$
14.25	$(\overline{12}\ 3\ 0)$	12.68	$(\overline{1}\ 0\ 15)$	11.42	$(0\ 3\ \overline{25})$
18.93	$(\overline{3}\ 1\ 0)$	18.92	$(\overline{1}\ 0\ 10)$	22.62	$(0\ 6\ \overline{25})$
28.07	$(\overline{6}\ 3\ 0)$	22.62	$(\overline{3}\ 0\ 25)$	33.4	$(0\ 9\ \overline{25})$
36.87	$(\overline{3}\ 2\ 0)$	36.87	$(\overline{1}\ 0\ 5)$	57.22	$(0\ 36\ \overline{55})$
53.13	$(\overline{3}\ 3\ 0)$	45.24	$(\overline{1}\ 0\ 4)$	61.93	$(0\ 18\ \overline{25})$
90	$(\overline{3}\ 6\ 0)$	61.93	$(\overline{9}\ 0\ 25)$	67.38	$(0\ 4\ \overline{5})$
126.87	$(\overline{3}\ 12\ 0)$	79.61	$(\overline{1}\ 0\ 2)$	73.74	$(0\ 9\ \overline{10})$
136.4	$(\overline{3}\ 15\ 0)$	90	$(\overline{3}\ 0\ 5)$	90	$(0\ 6\ \overline{5})$
143.13	$(\overline{1}\ 6\ 0)$	126.87	$(\overline{6}\ 0\ 5)$	100.39	$(0\ 36\ \overline{25})$
151.93	$(\overline{3}\ 24\ 0)$	146.6	$(\overline{2}\ 0\ 1)$	112.62	$(0\ 9\ \overline{5})$
161.08	$(\overline{1}\ 12\ 0)$	161.08	$(\overline{18}\ 0\ 5)$	126.87	$(0\ 12\ \overline{5})$
198.93	$(\overline{1}\ \overline{12}\ 0)$	198.93	$(\overline{18}\ 0\ \overline{5})$	134.76	$(0\ 72\ \overline{25})$
208.07	$(\overline{3}\ \overline{24}\ 0)$	213.4	$(\overline{2}\ 0\ \overline{1})$	143.13	$(0\ 18\ \overline{5})$
216.87	$(\overline{1}\ \overline{6}\ 0)$	233.13	$(\overline{6}\ 0\ \overline{5})$	161.08	$(0\ 36\ \overline{5})$
223.6	$(\overline{3}\ \overline{15}\ 0)$	270	$(\overline{3}\ 0\ \overline{5})$	170.47	$(0\ 72\ \overline{5})$
233.13	$(\overline{3}\ \overline{12}\ 0)$	280.39	$(\overline{1}\ 0\ \overline{2})$	189.53	$(0\ \overline{72}\ \overline{5})$
270	$(\overline{3}\ \overline{6}\ 0)$	298.07	$(\overline{9}\ 0\ \overline{25})$	198.93	$(0\ \overline{36}\ \overline{5})$
306.87	$(\overline{3}\ \overline{3}\ 0)$	314.76	$(\overline{1}\ 0\ \overline{4})$	216.87	$(0\ \overline{18}\ \overline{5})$
323.13	$(\overline{3}\ \overline{2}\ 0)$	323.13	$(\overline{1}\ 0\ \overline{5})$	225.24	$(0\ \overline{72}\ \overline{25})$
331.93	$(\overline{6}\ \overline{3}\ 0)$	337.38	$(\overline{3}\ 0\ \overline{25})$	233.13	$(0\ \overline{12}\ \overline{5})$
341.08	$(\overline{3}\ \overline{1}\ 0)$	341.08	$(\overline{1}\ 0\ \overline{10})$	247.38	$(0\ \overline{9}\ \overline{5})$
345.75	$(\overline{12}\ \overline{3}\ 0)$	347.32	$(\overline{1}\ 0\ \overline{15})$	259.61	$(0\ \overline{36}\ \overline{25})$
350.47	$(\overline{6}\ \overline{1}\ 0)$	354.28	$(\overline{3}\ 0\ \overline{100})$	270	$(0\ \overline{6}\ \overline{5})$
				286.26	$(0\ \overline{9}\ \overline{10})$
				292.26	$(0\ \overline{4}\ \overline{5})$
				298.08	$(0\ \overline{18}\ \overline{25})$
				302.78	$(0\ \overline{36}\ \overline{55})$
				326.61	$(0\ \overline{9}\ \overline{25})$
				337.38	$(0\ \overline{6}\ \overline{25})$
				348.58	$(0\ \overline{3}\ \overline{25})$
				354.28	$(0\ \overline{3}\ \overline{50})$

Table 2: Studied surfaces related to STGBs of α-U.

type A		type B		type C	
tilting axis	$\langle 1\ 0\ 0\rangle$	tilting axis	$\langle 0\ 0\ 1\rangle$	tilting axis	$\langle 0\ 0\ 1\rangle$
tilt plane or cut plane	(0 1 0)	tilt plane or cut plane	(1 0 0)	tilt plane or cut plane	(0 1 0)
shear plane	(0 0 1)	shear plane	(0 1 0)	shear plane	(1 0 0)
misorientation angle (deg)	STGB plane	misorientation angle (deg)	STGB plane	misorientation angle (deg)	STGB plane
4.765	$(\overline{6}\ 1\ 0)$	2.86	$(\overline{3}\ 0\ 100)$	2.86	$(0\ 3\ \overline{50})$
7.125	$(\overline{12}\ 3\ 0)$	6.34	$(\overline{1}\ 0\ 15)$	5.71	$(0\ 3\ \overline{25})$
9.465	$(\overline{3}\ 1\ 0)$	9.46	$(\overline{1}\ 0\ 10)$	11.31	$(0\ 6\ \overline{25})$
14.035	$(\overline{6}\ 3\ 0)$	11.31	$(\overline{3}\ 0\ 25)$	16.7	$(0\ 9\ \overline{25})$
18.435	$(\overline{3}\ 2\ 0)$	18.435	$(\overline{1}\ 0\ 5)$	28.61	$(0\ 36\ \overline{55})$
26.565	$(\overline{3}\ 3\ 0)$	22.62	$(\overline{1}\ 0\ 4)$	30.965	$(0\ 18\ \overline{25})$
45	$(\overline{3}\ 6\ 0)$	30.965	$(\overline{9}\ 0\ 25)$	33.69	$(0\ 4\ \overline{5})$
63.435	$(\overline{3}\ 12\ 0)$	39.805	$(\overline{1}\ 0\ 2)$	36.87	$(0\ 9\ \overline{10})$
68.2	$(\overline{3}\ 15\ 0)$	45	$(\overline{3}\ 0\ 5)$	45	$(0\ 6\ \overline{5})$
71.565	$(\overline{1}\ 6\ 0)$	63.435	$(\overline{6}\ 0\ 5)$	50.195	$(0\ 36\ \overline{25})$
75.965	$(\overline{3}\ 24\ 0)$	73.3	$(\overline{2}\ 0\ 1)$	56.31	$(0\ 9\ \overline{5})$
80.54	$(\overline{1}\ 12\ 0)$	80.54	$(\overline{18}\ 0\ 5$	63.435	$(0\ 12\ \overline{5})$
99.465	$(\overline{1}\ \overline{12}\ 0)$	99.465	$(\overline{18}\ 0\ \overline{5})$	67.38	$(0\ 72\ \overline{25})$
104.035	$(\overline{3}\ \overline{24}\ 0)$	106.7	$(\overline{2}\ 0\ \overline{1})$	71.565	$(0\ 18\ \overline{5})$
108.435	$(\overline{1}\ \overline{6}\ 0)$	116.565	$(\overline{6}\ 0\ \overline{5})$	80.54	$(0\ 36\ \overline{5})$
111.8	$(\overline{3}\ \overline{15}\ 0)$	135	$(\overline{3}\ 0\ \overline{5})$	85.235	$(0\ 72\ \overline{5})$
116.565	$(\overline{3}\ \overline{12}\ 0)$	140.195	$(\overline{1}\ 0\ \overline{2})$	94.765	$(0\ \overline{72}\ \overline{5})$
135	$(\overline{3}\ \overline{6}\ 0)$	149.035	$(\overline{9}\ 0\ \overline{25})$	99.465	$(0\ \overline{36}\ \overline{5})$
153.435	$(\overline{3}\ \overline{3}\ 0)$	157.38	$(\overline{1}\ 0\ \overline{4})$	108.435	$(0\ \overline{18}\ \overline{5})$
161.565	$(\overline{3}\ \overline{2}\ 0)$	161.565	$(\overline{1}\ 0\ \overline{5})$	112.62	$(0\ \overline{72}\ \overline{25})$
165.965	$(\overline{6}\ \overline{3}\ 0)$	168.69	$(\overline{3}\ 0\ \overline{25})$	116.565	$(0\ \overline{12}\ \overline{5})$
170.54	$(\overline{3}\ \overline{1}\ 0)$	170.54	$(\overline{1}\ 0\ \overline{10})$	123.69	$(0\ \overline{9}\ \overline{5})$
172.875	$(\overline{12}\ \overline{3}\ 0)$	173.66	$(\overline{1}\ 0\ \overline{15})$	129.805	$(0\ \overline{36}\ \overline{25})$
175.235	$(\overline{6}\ \overline{1}\ 0)$	177.14	$(\overline{3}\ 0\ \overline{100})$	135	$(0\ \overline{6}\ \overline{5})$
				143.13	$(0\ \overline{9}\ \overline{10})$
				146.13	$(0\ \overline{4}\ \overline{5})$
				149.04	$(0\ \overline{18}\ \overline{25})$
				151.39	$(0\ \overline{36}\ \overline{55})$
				163.305	$(0\ \overline{9}\ \overline{25})$
				168.69	$(0\ \overline{6}\ \overline{25})$
				174.29	$(0\ \overline{3}\ \overline{25})$
				177.14	$(0\ \overline{3}\ \overline{50})$

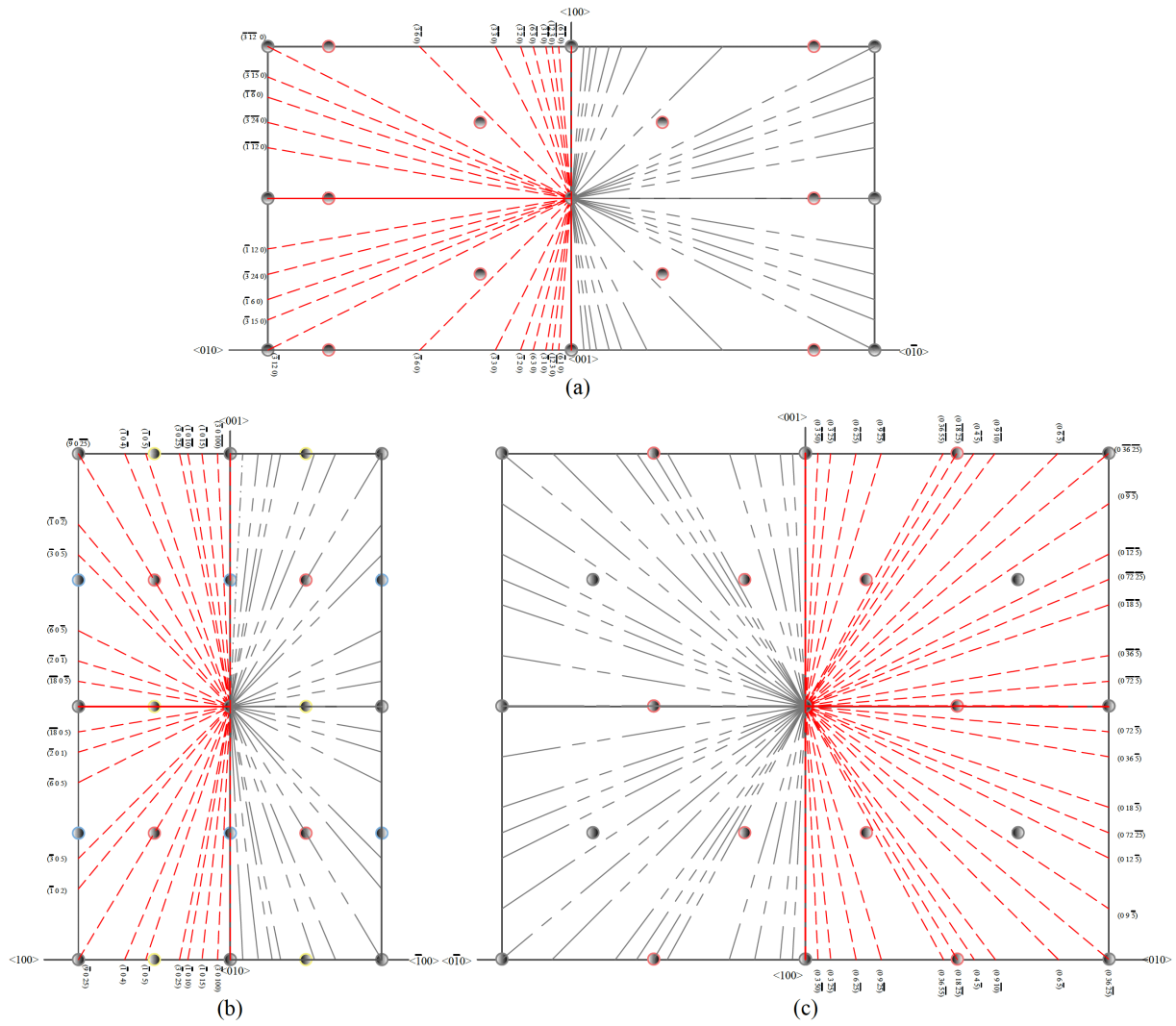

Figure 10: Schematic diagram of symmetric tilt grain boundaries (STGB) of (a) type A, (b) type B and (c) type C along with the supercell axis. In each diagram four unit cells are shown, with gray colored planes (large dash) the mirror image of red colored planes (small dash) of the α-U lattice. To illustrate the misorientation angles in a sequential manner, here the authors have shifted the planes (keeping their tilt angle with tilting plane same) to the same lattice point.